Numerical antiresonance continuation of structural systems

A. Renault [a,b,*], O. Thomas [a], H. Mahé [b]

[a] Arts et Métiers ParisTech, LISPEN EA 7515, 8 bd. Louis XIV, 59046 Lille, France
[b] Valeo Transmissions, Centre d'Étude des Produits Nouveaux Espace Industriel Nord, Route de Poulainville, 80009 Amiens Cedex 1, France

A B S T R A C T

Tuned dynamic absorbers are usually used to counteract vibrations at a given frequency. Presence of non-linearities causes energy-dependent relationship of their resonance and antiresonance frequencies at large amplitude of motion, which consequently leads to a detuning of the absorber from the targeted frequency. This paper presents a procedure to track an extremum point (minimum or maximum) of nonlinear frequency responses, based on a numerical continuation technique coupled to the harmonic balance method to follow periodic solutions in forced steady-state. It thus enable to track a particular antiresonance. The procedure is tested and applied on some application cases to highlight the resonance and antiresonance behavior in presence of geometrically non-linear and/or inertial interactions.

1. Introduction

In the widely investigated domain of attenuation of vibrations [1], passive tuned vibration absorbers are usually a suitable choice. To overcome the low robustness of linear absorbers, based on the Frahm's damper concept [2], nonlinear ones have been proposed. We can gather them into two families. The first one is the class of non linear tuned vibration absorbers (NLTVA). Those devices are based on the concept, introduced in [3], that the nonlinear absorber should possess a frequency-energy dependence identical to that of the nonlinear host system. Among other studies on the subject, [4] proposes a generalization of DenHartog's equal-peak method to non linear systems and gives a methodology to tune the whole nonlinear restoring force of the NLTVA on that of the primary structure of interest. The second class of absorbers is the one of so-called nonlinear energy sinks (NES) [5,6]. They exploit a secondary oscillator designed with strong non-linearities. Several ideas have bean proposed. Among others, one can cite essential cubic stiffness [7], non-polynomial non-linearities [8], vibro-impact devices [9].

For some applications, the nonlinear nature of the absorber is a constraint imposed by the design itself. For example, the so-called centrifugal pendulum vibration absorber (CPVA) used by the automotive industry to counteract irregularities of rotation of powertrains is intrinsically nonlinear. This passive device evolves in a centrifugal acceleration field and consists of a set of pendular oscillators (the CPVAs) acting as dynamic absorbers on a rotating primary structure [10–12]. Behavior of pendular oscillators is known to be sensitive to the path shape followed by their center of mass which involves geometric non-linearities at large amplitude of motion. Circular path causes a softening behavior while the so-called tautochronic path (from Greek: *tauto*, same, and *chrono*, time) keeps frequency independent of the motion amplitude [13]. For example, tautochrone curves in gravitational and centrifugal acceleration fields are respectively the cycloid [14] and the epicycloid [15].

When CPVAs are coupled to the primary structure, the system is subject to strong nonlinear inertial coupling between host structure and absorbers. This additional source of non-linearities re-activates the frequency-energy dependence even if the oscillator has been designed to be tautochronous. The result is the detuning of the CPVA and the shifting of the optimal operating frequency (an antiresonance of the whole system) from the targeted tuning frequency. For such applications, the knowledge of the antiresonance behavior is essential.

The study of the response of a nonlinear dynamic system can be dealt with through analytical or numerical approaches. The first category is particularly suitable for a parametric study of systems having few degrees of freedom. One can cite the Lindstedt-Poincaré method or multiple time scales method [16] for example. Although those methods give an analytical approximation of the solution, most of them assume that the effect of the non-linearity is small, which becomes invalid for a large amplitude of motion. From a numerical point of view, there is a large variety of methods. Best known are direct time integration procedures of the governing equations. They are usually easy to implement and deployed in many commercial softwares. However, they may require extensive computation time to reach the steady state in case of long transient and don't give informations on the unstable solutions. An other class of numerical methods is the periodic steady-state analysis. One can cite the shooting method [17] that allows to directly reach a periodic steady-state through an iterative correction of the initial conditions up to the basin of attraction of periodic solutions. Some other methods are based on a discretization of the periodic solution through an expansion as a linear combination of known functions. For instance, the orthogonal collocation method adopts a piecewise polynomial representation of the solution [18]. In the frequency domain, the so-called harmonic balance method (HBM), used in this paper, is very popular and consists in discretizing the unknown solution by means of a truncated Fourier series [16].

In practice, it is often convenient to compute branches of steady-state periodic solutions as a function of a given parameter (amplitude, frequency, ...), leading to numerical continuation methods. Most common procedures are surely those based on a predictor corrector method with arc length parametrization, implemented for example in AUTO [19] or MATCONT [20] softwares. Another approach, the so-called asymptotic numerical method (ANM), addressed in the following of this paper, is based on a high order predictor method without correction and adopts an analytical representation of the branch of solution [21].

Prediction of an extremum of nonlinear frequency response is often helpful for the design of nonlinear systems. For instance, Habib and Kerschen use in Ref. [22] a perturbation method coupled to the HBM in order to analytically predict resonance peaks and establish some design rules about of the NLTVA. Some numerical methods are proposed to accurately predict amplitude resonance peak of a nonlinear system. For instance, Liao et al. use optimization procedure coupled to the HBM to obtain the worst periodic vibration response amplitude [23]. The case of quasi-periodic oscillations with uncertainties has been dealt in Ref. [24].

The contribution of this paper is to propose a general method to follow periodic solutions at a particular point of a dynamic response, namely an extremum (minimum as well as maximum) of a particular nonlinear frequency response of the system. Since an antiresonance can be defined as a particular minimum, our procedure is able to track antiresonances. It is also able to track resonance points, defined as a maximum of a frequency response. Our contribution provides an additional tool for the development of dynamic absorbers, in addition to particular procedures such as bifurcation tracking methods [25,26]. In this article, we have implemented our strategy of continuation of extrema in the framework of the ANM/HBM and the software Manlab2.0 [27], but since it is very close to fold bifurcation continuation, it could also be implemented in generic continuation solvers like AUTO [19] and MATCONT [20].

Stability of the solution is an essential aspect and must be considered during design phase of nonlinear systems. In particular, there can exist conditions where the desired response can be unstable near antiresonance [28,29]. However, the authors want to keep the focus of the paper on extremum tracking procedure and stability of the response is not addressed.

This paper is organized as follows: Section 2 introduces the framework of the study and the concept of antiresonance is extended from linear to nonlinear scope. The formulation of the antiresonance continuation is addressed in Section 3 and its numerical solving with the asymptotic numerical method in Section 4. Then, the methodology is applied on the so-called Euler's pendulum which exhibits non-linearities of various nature. Finally, the conclusion is outlined in the last section.

2. General framework and antiresonance concept

In this section, we establish the framework of the study through the highlighting of some fundamental concepts faced by N_{eq} degrees-of-freedom dynamical systems governed by:

$$\boldsymbol{M}\ddot{\boldsymbol{x}} + \boldsymbol{D}\dot{\boldsymbol{x}} + \boldsymbol{K}\boldsymbol{x} + \boldsymbol{f}_{nl}(\boldsymbol{x}, \dot{\boldsymbol{x}}) = \boldsymbol{F}\cos\omega t, \tag{1}$$

where $(\dot{-})$ stands for the derivative of $(-)$ w.r.t. the time t, $\boldsymbol{x}$ is the vector of unknowns, $\boldsymbol{M}$ is the mass matrix, $\boldsymbol{D}$ is the damping matrix, $\boldsymbol{K}$ is the stiffness matrix, $\boldsymbol{f}_{nl}(\boldsymbol{x}, \dot{\boldsymbol{x}})$ is the vector of nonlinear forces that depends on $\boldsymbol{x}$ and $\dot{\boldsymbol{x}}$ and $\boldsymbol{F}$ is the vector of external forces.

In order to illustrate the concepts introduced in this section, we consider the two degrees of freedom Duffing-like system depicted on Fig. 1. It is composed of two oscillators. The first one of mass m_1, subjected to an external force $f\cos\omega t$, is linked to the Galilean frame through a linear stiffness k_1 and a linear viscous damping c_1. Amplitude of oscillations of m_1 is measured by the degree of freedom x_1. The second oscillator, of mass m_2, is coupled to the primary one through a linear stiffness

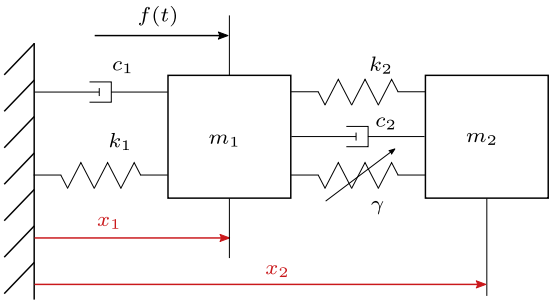

Fig. 1. Duffing-like system.

k_2 and a viscous damping c_2. In addition, both oscillators are coupled through a cubic non linear stiffness whose magnitude is governed by the coefficient γ. Amplitude of oscillations of m_2 is monitored by the degree of freedom x_2. The equations of motion are:

$$\begin{cases} m_1\ddot{x}_1 + c_1\dot{x}_1 + c_2\left(\dot{x}_1 - \dot{x}_2\right) + k_1 x_1 + k_2\left(x_1 - x_2\right) + \gamma\left(x_1 - x_2\right)^3 = f\cos\omega t, & (2) \\ m_2\ddot{x}_2 + c_2\left(\dot{x}_2 - \dot{x}_1\right) + k_2\left(x_2 - x_1\right) + \gamma\left(x_2 - x_1\right)^3 = 0. & (3) \end{cases}$$

These equations are obviously of the form of the general model (1).

2.1. Antiresonance: the linear point of view, $\boldsymbol{f}_{nl}(\boldsymbol{x}, \dot{\boldsymbol{x}}) = 0$

We address the underlying linear system described by Eq. (1), *i.e.* with $\boldsymbol{f}_{nl}(\boldsymbol{x}, \dot{\boldsymbol{x}}) = 0$. Solutions are assumed of the form of

$$x_i(t) = \mathrm{Re}\{\hat{x}_i e^{j\omega t}\}, \tag{4}$$

where the subscript i stands for the ith degree of freedom and j is the imaginary unit. Moreover, we consider the vector of external forces of the form $\boldsymbol{F} = [0 \cdots f_k \cdots 0]^\intercal$, where f_k is the amplitude of excitation of the kth degree of freedom. The frequency response functions (FRF) $H_{ik}(\omega)$ are given by

$$H_{ik}(\omega) = \left|\frac{\hat{x}_i(\omega)}{f_k}\right|. \tag{5}$$

Several particular frequencies can be classically defined as follows:

The eigenfrequencies ω_n. Eigenfrequencies are global features of the undamped and unforced system ($\boldsymbol{D} = 0, \boldsymbol{F} = 0$) and correspond to free oscillations frequencies. They are solutions of the following eigenproblem:

$$\left[\boldsymbol{K} - \omega_n^2 \boldsymbol{M}\right]\boldsymbol{\Phi}_n = \boldsymbol{0}, \tag{6}$$

where the subscript n stands for the nth mode so $\boldsymbol{\Phi}_n$ is the nth eigenvector. In forced vibrations ($\boldsymbol{F} \neq 0$), those eigenfrequencies ω_n are exactly obtained when the response $\boldsymbol{x}(t)$ oscillates synchronously, in phase quadrature with the harmonic excitation $\boldsymbol{F}$ (phase resonance) [30]. If there is no damping ($\boldsymbol{D} = 0$), the phase resonance coincides with the amplitude resonance, which is in this case infinite and the eigenfrequencies correspond to the poles of the FRFs (the zeros of their denominator).

The resonance frequencies ω_{Rn}. For a conservative system ($\boldsymbol{D} = 0$), as recalled above, their exist amplitude resonances for each eigenfrequency ω_n, for which the amplitude of all the FRFs $H_{ik}, \forall i, k$ (except if i or k correspond to a node of the corresponding mode shape) is infinite. The amplitude resonances are thus a global features of the forced system ($\boldsymbol{F} \neq 0$). For a lightly damped system, the amplitude resonances correspond to maximums of the FRFs (for resonances for which the modal damping is undercritical), that occur for frequencies ω_{Rn} slightly different from ω_n, but very close. They are also slightly different from one FRF to the other.

The antiresonance frequencies ω_{ARp}. For a conservative system ($\boldsymbol{D} = 0$), there exist particular frequencies $\omega_{ARp}, p \in \mathbb{N}^*$, called antiresonances, for which the frequency responses are zero: $H_{ik}(\omega_{ARp}) = 0$. They are local features of the forced system ($\boldsymbol{F} \neq 0$) and depend on given driving point k and measurement point i. In particular, the driving point frequency responses $H_{ii}(\omega)$ shows an antiresonance between each successive resonance [30]. They correspond to the zeros of the FRFs (zeros of their numerator). Physically, if an antiresonance occurs for the frequency response of a particular degree of freedom d, namely $H_{dk}(\omega_{AR}) = 0$, it means that the system oscillates in order to exactly cancel the forces applied to the degree of freedom d. It can also be shown that the antiresonance frequencies ω_{ARp} associated to a given FRF H_{ij} correspond to the eigenfrequencies of a dual system, obtained by imposing $x_i \equiv 0$ or $x_j \equiv 0$ [31,32].

In damped vibrations, strict antiresonances does not exist since there is no frequencies for which the FRFs vanish. However, increasing the damping from zero, one can show that the above defined antiresonance of the undamped system (zeros of the FRFs) become minimums of the FRFs. However, the FRFs shows other minimums which are not antiresonances, since they don't correspond to zeros of the undamped FRFs. Consequently, any minimum of a given FRF is not necessarily an antiresonance.

To illustrate the concept underlined above, we consider the underlying linear system described by Eqs. (2) and (3). Viscous damping coefficients c_1 and c_2 are assumed to be equal *i.e.*, $c_1 = c_2 = c$ and solutions in term of x_1 and x_2 are assumed of the form of (4). Frequency response functions of the system, depicted on Fig. 2, are given by

$$H_{11}(\omega) = \frac{\hat{x}_1}{f_1} = \frac{k_2 - m_2\omega^2 + jc\omega}{D(\omega)} \quad \text{and} \quad H_{21}(\omega) = \frac{\hat{x}_2}{f_1} = \frac{k_2 + jc\omega}{D(\omega)}, \tag{7}$$

where

$$D(\omega) = m_1 m_2^2 \omega^4 - jc(m_1 + 2m_2)\omega^3 - \left(m_1 k_2 + m_2(k_1 + k_2) + c^2\right)\omega^2 + jc(k_2 + k_1)\omega + k_1 k_2. \tag{8}$$

According to Eq. (6), eigenfrequencies and eigenvectors can be written

$$\omega_1 = \frac{k_1 + 2k_2 - \sqrt{k_1^2 + 4k_2}}{2m} \quad \text{and} \quad \Phi_1 = \left[\frac{\sqrt{k_1^2 + 4k_2^2} - k_1}{2k_2} \quad 1\right]^{\mathsf{T}}, \tag{9}$$

where $m_1 = m_2 = m$, for the first in phase motion mode and

$$\omega_2 = \frac{k_1 + 2k_2 + \sqrt{k_1^2 + 4k_2}}{2m} \quad \text{and} \quad \Phi_2 = \left[-\frac{\sqrt{k_1^2 + 4k_2^2} + k_1}{2k_2} \quad 1\right]^{\mathsf{T}}, \tag{10}$$

for the second phase opposition motion mode.

As theoretically explained above, both FRFs of Eq. (7) share the same denominator $D(\omega)$ that vanishes, for the conservative system ($c = 0$), at eigenfrequencies ω_1 and ω_2 so $H_{i1}(\omega_i), i = 1, 2$ is infinite (global features). For the damped system, H_{i1} is maximal but finite for the two resonance frequencies ω_{R1} and ω_{R2}, close to ω_1 and ω_2.

Antiresonance frequencies of the conservative system are roots of numerators of H_{i1} with $c = 0$. Here, only H_{11} vanishes at a particular frequency:

$$\omega_{AR} = \omega_{02} = \sqrt{\frac{k_2}{m_2}}. \tag{11}$$

It is a local feature of $H_{ii}(\omega)$ and it correspond to the eigenfrequency ω_{02} of the dual system, obtained by keeping the first degree of freedom immovable ($x_1(t) \equiv 0$). It correspond to the secondary oscillator, that acts then as a vibration damper on the primary one. In the presence of damping, H_{11} is minimal but non zero, $\omega_{AR1} \neq \omega_{02}$. Also, the local minimum shown on H_{21} is not an antiresonance.

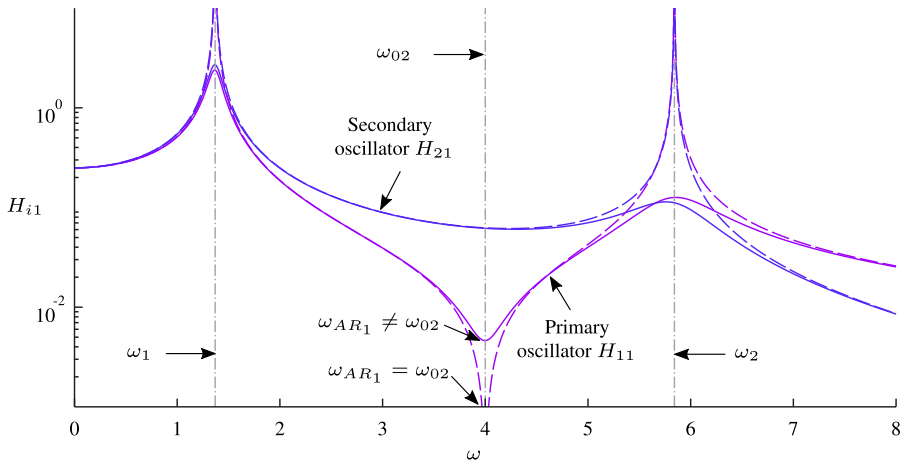

Fig. 2. Frequency response functions of the underlying linear system. Solid lines denote damped response *i.e.*, $c \neq 0$, dashed lines stand for the undamped response *i.e.*, $c = 0$ and dashed-doted lines represent the locus of eigenfrequencies. Parameter values: $m_1 = m_2 = 1,\ k_1 = 4,\ k_2 = 16,\ c = 0.3$.

2.2. Antiresonance: the non linear point of view: $\boldsymbol{f}_{nl}(\boldsymbol{x},\dot{\boldsymbol{x}}) \neq 0$

This section aims to see how linear concepts recalled in Section 2.1 about antiresonances can be extended to the nonlinear case. To deal with the nonlinear behavior of the system conveniently, we need to enhance the representation of the solution assumed before through Eq. (4). For this, the solution is still assumed periodic but approximated by a truncated Fourier series:

$$\boldsymbol{x}(t) = \boldsymbol{x}^0 + \sum_{j=1}^{H} \boldsymbol{x}^{cj} \cos j\omega t + \boldsymbol{x}^{sj} \sin j\omega t, \tag{12}$$

where H is the number of harmonics retained in the solution and the subscript j stands for the jth harmonic. For instance, in the case of the system depicted in Fig. 1, one can write $\boldsymbol{x}(t) = [x_1(t)\ x_2(t)]^\intercal$, $\boldsymbol{x}^0 = \left[x_1^0\ x_2^0\right]^\intercal$, $\boldsymbol{x}^{cj} = \left[x_1^{cj}\ x_2^{cj}\right]^\intercal$ and $\boldsymbol{x}^{sj} = \left[x_1^{sj}\ x_2^{sj}\right]^\intercal$. Following the harmonic balance method [16], the periodic approximation is substituted into the equations of motion and harmonic terms higher than H, arising from non-linearities, are neglected since they are not taken into account in (12). We are interested by periodic solutions in the steady state, coefficients of each harmonic are then equated to zero. A non linear algebraic system is obtained, of the form:

$$\boldsymbol{R}(\boldsymbol{U},\omega,f) = \boldsymbol{0}, \tag{13}$$

where the vector of $N_{eq}(2H+1)$ unknowns is $\boldsymbol{U} = \left[\boldsymbol{x}^0\ \boldsymbol{x}^{cj}\ \boldsymbol{x}^{sj}\ \ldots\ \boldsymbol{x}^{cH}\ \boldsymbol{x}^{sH}\right]^\intercal$. In the following, the modulus of the jth harmonic of the response measured at the ith degree of freedom will be denoted by

$$|x_i|^{Hj} = \sqrt{x_i^{cj\,2} + x_i^{sj\,2}} \tag{14}$$

Dual system. We first focus on the forced response of the dual system (the secondary oscillator), obtained by imposing $x_1 \equiv 0$ in Eqs. (2) and (3). The governing equation can be written:

$$m_2\ddot{x}_2 + c_2\dot{x}_2 + k_2x_2 + \gamma x_2^3 = f\cos\omega t. \tag{15}$$

This equation is a Duffing oscillator [33] whose non linear nature arises from the nonlinear part of the stiffness γx_2^3. This section recalls some basic features of the Duffing oscillator that will be useful in the following. All curves of upcoming Figs. 3–5 were obtained by continuation methods addressed in Section 3. According to the sign of γ, the oscillator stiffness decreases ($\gamma < 0$) or increases ($\gamma > 0$) as the amplitude of oscillation grows. Both cases are illustrated on Fig. 3. Frequency denoted $\omega_{02_{NL}}$ describes the backbone curve, the skeleton of the forced response, and represents the free oscillation frequency of the underlying unforced ($f = 0$) and undamped ($c_2 = 0$) system. Because of the curvature of the backbone, multivalued regimes appear with unstable solutions. Stable and unstable solutions are connected by a fold (saddle node) bifurcation, characterized by a limit w.r.t. ω (vertical tangency).

Fig. 4 shows the evolution of the hardening response as the amplitude of the external force increases. One can see that the fold bifurcation appears beyond a given amplitude of motion and its tracking (see [25,26] and Section 3.2), depicted by the dashed line, is useful to predict for instance the critical value of the force amplitude from which the jump phenomenon occurs.

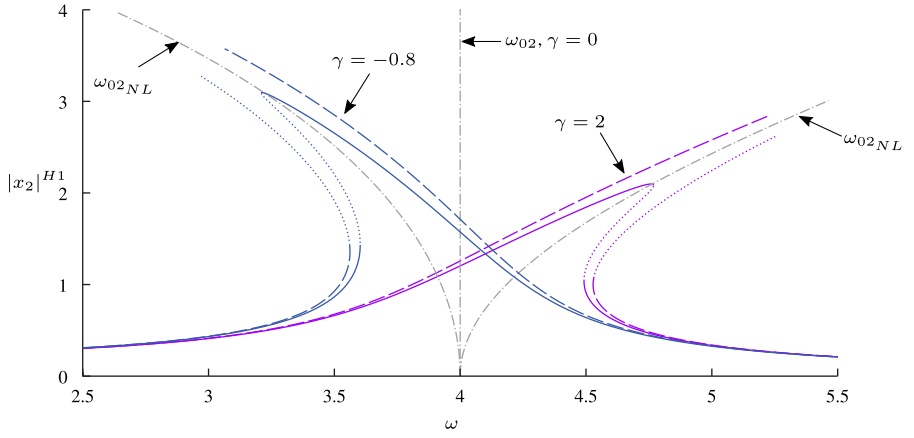

Fig. 3. Forced response of the secondary oscillator for two values of γ. Solid lines denote damped response *i.e.*, $c_2 \neq 0$, dashed lines stand for the undamped response *i.e.*, $c_2 = 0$, dotted lines show the unstable solutions and backbone curves are dashed-doted lines. Parameter values: $m_2 = 1$, $k_2 = 16$, $c_2 = 0.3$, $f = 3, H = 10$.

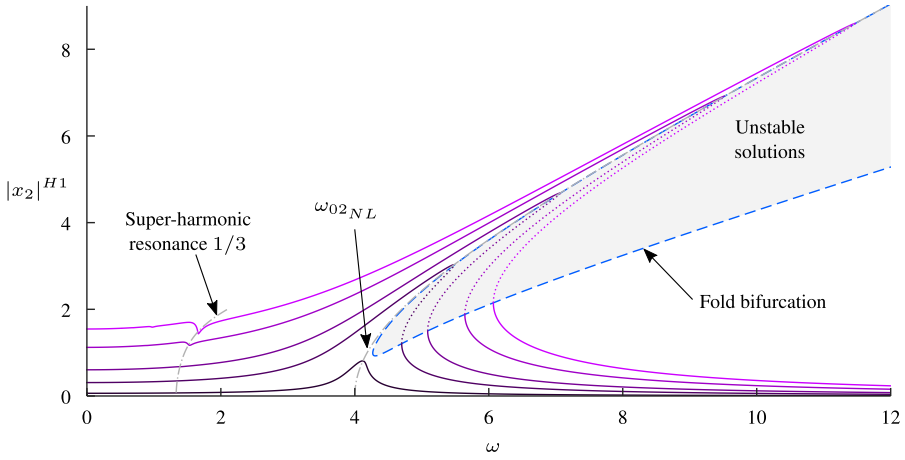

Fig. 4. Forced response of the secondary oscillator ($\gamma = 2$) as the driving force increases. Dashed line stands for the the locus of the fold bifurcation, dotted lines show the unstable solutions and backbone curves are dashed-doted lines. Parameter values: $m_2 = 1,\ k_2 = 16,\ c_2 = 0.3,\ f = [1\ 5\ 10\ 20\ 30],\ H = 10$.

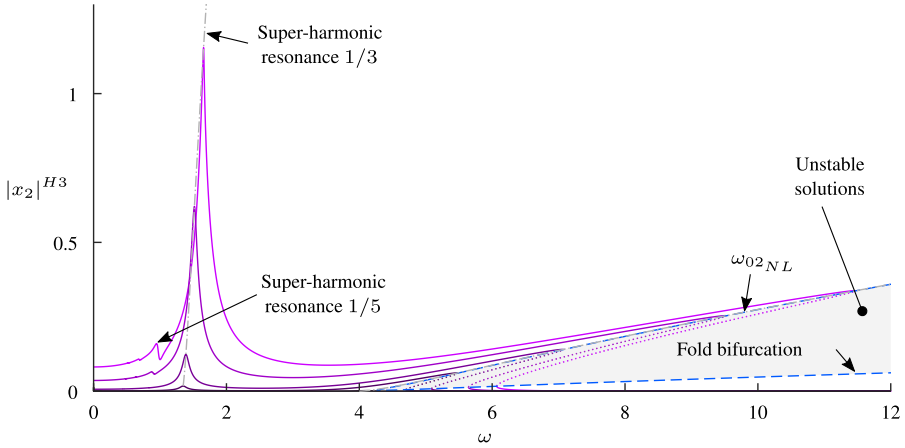

Fig. 5. Forced response of the secondary oscillator ($\gamma = 2$) as the driving force increases. Dashed line stands for the the locus of the fold bifurcation, dotted lines show the unstable solutions and backbone curves are dashed-doted lines. Parameter values: $m_2 = 1,\ k_2 = 16,\ c_2 = 0.3,\ f = [1\ 5\ 10\ 20\ 30],\ H = 10$.

An other basic feature of non linear systems is the harmonic distortion. Although the oscillator is subjected to a mono-harmonic excitation, its response is a superposition of harmonic components of the form of (12). Fig. 5 depicts the evolution of the third harmonic of the response as the amplitude of driving force increases. In the case of the Duffing oscillator, the non-linearity is an odd function so the even harmonic components are null, except if symmetry breaking bifurcations occur [34]. A relevant feature can be observed on Figs. 4 and 5 and denoted as *super-harmonic* resonance. Since the third harmonic oscillates at frequency three times higher than the driving force, it will excites the primary resonance at a frequency three time lower than the driving frequency. It is a super-harmonic resonance of order 3 and it is worth noting that its backbone is that of the primary resonance whose the frequency has been divided by 3. Following the same logic, one sees the super-harmonic resonance of order 5 growing up on Fig. 5. It is important to point out that, for responses shown here, approximation of the solution has been truncated to an order $H = 10$. If we chose an harmonic representation of the solution *i.e.*, $H = 1$, higher harmonic components would have been neglected in the total response. Accuracy of the harmonic balance method is conditioned to the fact that the Fourier series is rich enough and therefore depends on the number of harmonics retained in (12).

Coupled system. The full non linear system described by Eqs. (2) and (3) is now addressed. Fig. 6 depicts the first and the third harmonic of the forced response in the case of the softening system, whereas the hardening case is shown on Fig. 7.

This system has two nonlinear modes, corresponding to the in phase and phase opposition motion at small (linear) amplitude, since the mode shapes of nonlinear systems depend on the amplitude of oscillation [17]. Note the qualitative difference of behavior of the in phase and phase opposition modes. For the first one, the contribution of the non linear term γx_2^3 is very weak due to the in phase motion. For the second mode, the phase opposition motion, the non linear stiffness is involved so this mode captures the softening/ hardening behavior of the secondary oscillator.

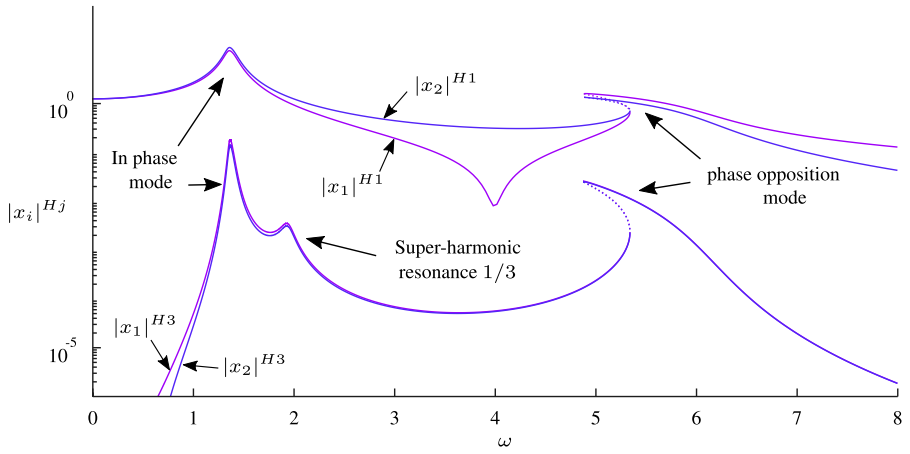

Fig. 6. Forced responses $|x_i|^{Hj}$ of the softening system. Solid lines denote stable solutions and dotted lines show the unstable solutions. Parameter values: $m_1 = m_2 = 1,\ k_1 = 4,\ k_2 = 16,\ c_1 = 0.3,\ c_2 = 0.1,\ \gamma = -0.8,\ f = 5,\ H = 10$.

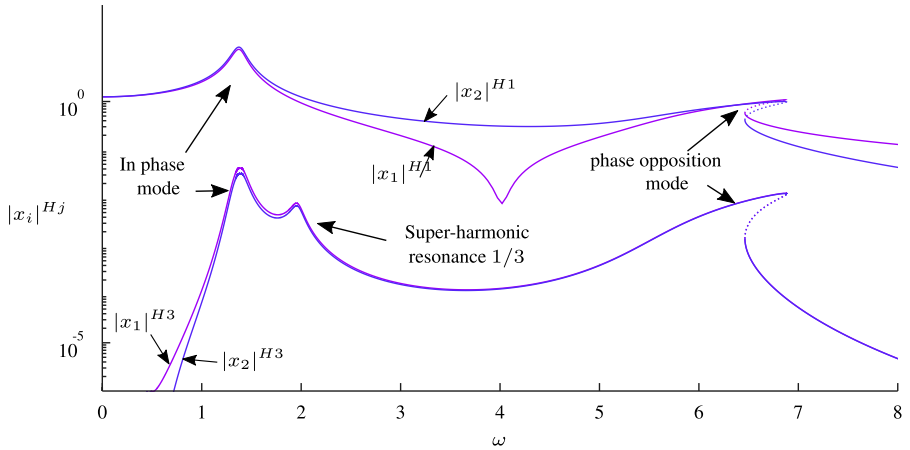

Fig. 7. Forced responses $|x_i|^{Hj}$ of the hardening system. Solid lines denote stable solutions and dotted lines show the unstable solutions. Parameter values: $m_1 = m_2 = 1,\ k_1 = 4,\ k_2 = 16,\ c_1 = 0.3,\ c_2 = 0.1,\ \gamma = 2,\ f = 5,\ H = 10$.

As stated in Section 2.1, the antiresonance is visible on the response of the primary oscillator, but, because of the non-linearities, only on $|x_1|^{H1}$. Indeed, at the antiresonance frequency, the first harmonic component of the net acting force on the primary mass is minimal (depending on the damping) since the restoring force of the secondary oscillator balances the driving force. This is not the case for higher harmonics because the driving force is of the form $f\cos\omega t$. The local minimum shown on the third harmonic is then not an antiresonance.

A focus at the vicinity of the antiresonance is given for damped softening and hardening systems on Figs. 8 and 9 respectively. Conservative cases are depicted in Figs. 10 and 11 and corresponding 3D representations are given in Fig. 12. One observes that antiresonance frequency is clearly impacted by non-linearities, since it depends on the amplitude of forcing. For conservative systems, antiresonance remains in the (ω,f) frequency-excitation amplitude planeof the 3D plots of Fig. 12, since $|x_1|^{H1}$ is strictly zero at this point. In the damped case, the antiresonance point moves out of the (ω,f) frequency-excitation amplitude plane as the driving force increases: the amplitude $|x_1|^{H1}$ is a minimum, but not a zero. In addition, it is worth noting that the topology of the branch of solution at the antiresonance point is inherently different between both cases. Without damping, the branch of solution of $|x_1|^{H1}$ is an angular point with an undefined tangency. For the damped case, the antiresonance is a minimum of $|x_1|^{H1}$ with an horizontal tangency in the $(\omega, |x_1|^{H1})$ frequency amplitude plane. In addition, it is worth noting that the topology of the branch of solution at the antiresonance point is inherently different between damped and conservatives cases. Without damping, the branch of solution of $|x_1|^{H1}$ is an angular point with an undefined tangency. For the damped case, the antiresonance is a minimum of $|x_1|^{H1}$ with an horizontal tangency in the $(\omega, |x_1|^{H1})$ frequency amplitude plane.

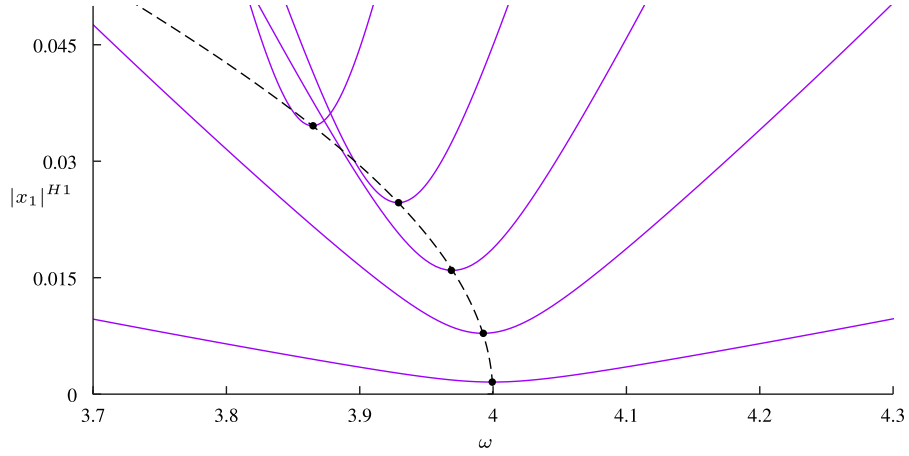

Fig. 8. Forced response $|x_1|^{H1}$ at the vicinity of the antiresonance of the softening system, dashed line is the locus of the antiresonance. Each curve corresponds to a given value of the forcing amplitude f ($f = [1\ 5\ 10\ 15\ 20]$). Parameter values: $m_1 = m_2 = 1,\ k_1 = 4,\ k_2 = 16,\ c_1 = 0.3,\ c_2 = 0.1,\ \gamma = -0.8,\ H = 10$.

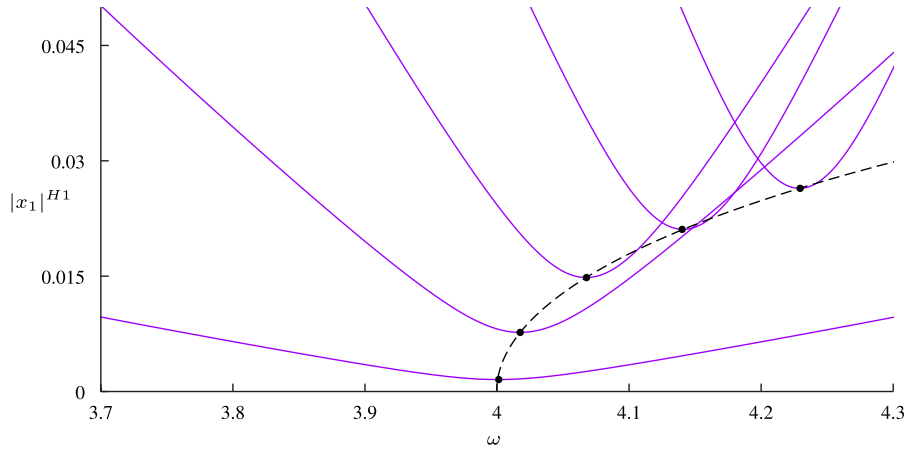

Fig. 9. Forced responses $|x_1|^{H1}$ at the vicinity of the antiresonance of the hardening system, dashed line is the locus of the antiresonance. Each curve corresponds to a given value of the forcing amplitude f ($f = [1\ 5\ 10\ 15\ 20]$). Parameter values: $m_1 = m_2 = 1,\ k_1 = 4,\ k_2 = 16,\ c_1 = 0.3,\ c_2 = 0.1,\ \gamma = 2,\ H = 10$.

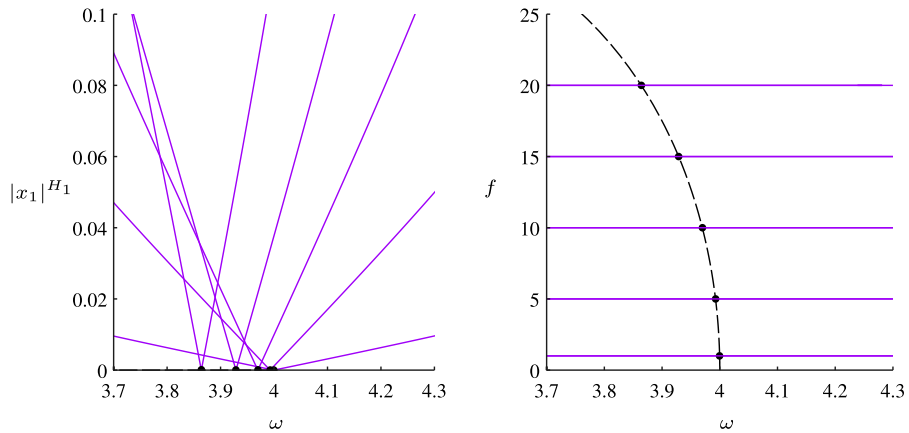

Fig. 10. Forced response $|x_1|^{H1}$ at the vicinity of the antiresonance of the conservative softening system, dashed line is the locus of the antiresonance. Representation in frequency – response amplitude plane; each curve corresponds to a given value of the forcing amplitude f ($f = [1\ 5\ 10\ 15\ 20]$) (left). Representation in frequency – excitation amplitude plane (right). Parameter values: $m_1 = m_2 = 1,\ k_1 = 4,\ k_2 = 16,\ c_1 = c_2 = 0,\ \gamma = -0.8,\ H = 10$.

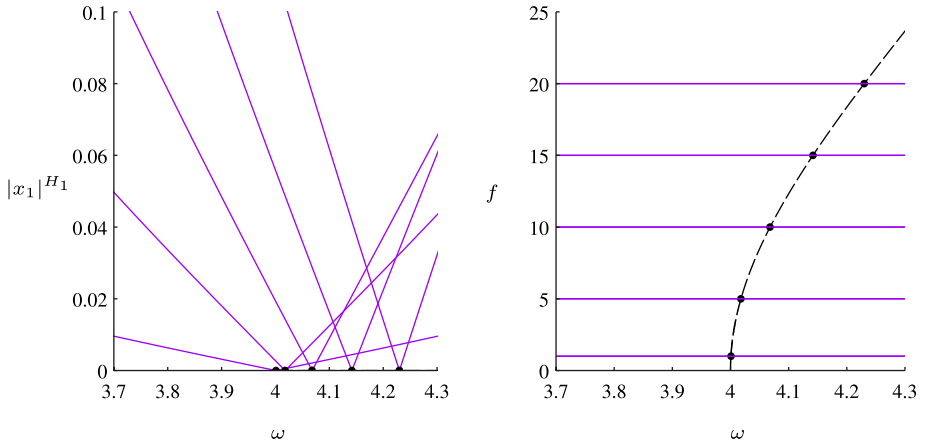

Fig. 11. Forced response $|x_1|^{H1}$ at the vicinity of the antiresonance of the conservative hardening system, dashed line is the locus of the antiresonance. Representation in frequency – response amplitude plane; each curve corresponds to a given value of the forcing amplitude f ($f = [1\ 5\ 10\ 15\ 20]$). (left). Representation in frequency – excitation amplitude plane (right). Parameter values: $m_1 = m_2 = 1,\ k_1 = 4,\ k_2 = 16,\ c_1 = c_2 = 0,\ \gamma = -0.8,\ H = 10$.

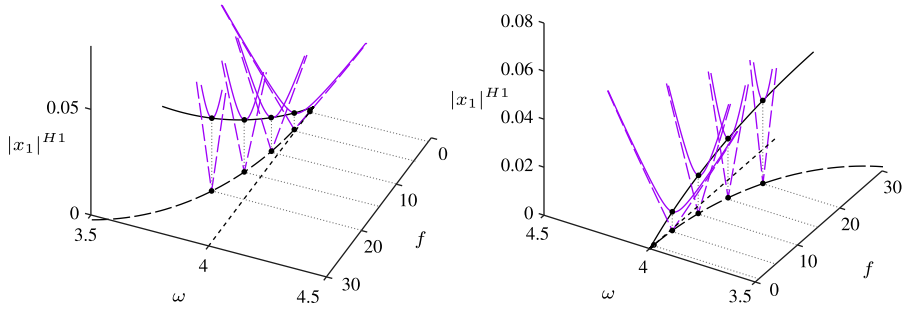

Fig. 12. 3D representation of the forced response $|x_1|^{H1}$ at the vicinity of the antiresonance of the softening system. Dashed lines correspond to conservative system ($c_1 = c_2 = 0$) and solid lines stand for the damped system ($c_1 = 0.3,\ c_2 = 0.1$). Each curve corresponds to a given value of the forcing amplitude f ($f = [5\ 10\ 15\ 20]$). Parameter values: $m_1 = m_2 = 1,\ k_1 = 4,\ k_2 = 16,\ \gamma = -0.8,\ H = 10$.

This amplitude-dependent behavior of the antiresonance can be surprising. Indeed, since the amplitude $|x_1|^{H1}$ is very small (zero in the case of a conservative system as stated above), one could think that the effect of nonlinearities is negligible. However, even if $|x_1|^{H1}$ is very small, all the other degrees of freedom and harmonics are not small and are responsible of this nonlinear behavior. In particular, $(x_1 - x_2)$ is not zero, which is related to the nonlinearities in Eqs. (2) and (3).

This amplitude-dependent behavior of the antiresonance frequency can be damaging. Let us imagine that the secondary oscillator has been designed, from the linear point of view, so that the antiresonance occurs at a given operating frequency. This is valid for small oscillations but when amplitude of motion grows the expected optimal operating frequency (antiresonance frequency) is not the effective operating frequency. Prediction of the antiresonance frequency as a function of amplitude of motion can then only be done on the couple system. In addition, because of amplitude-frequency dependence of the backbone curve, a comparison between the antiresonance frequency and the eigenfrequency of the dual system is impossible. To avoid redundant forced response simulations we propose to compute the locus of the antiresonance directly through a numerical continuation procedure, described in the following, as depicted by dashed lines on Figs. 8 and 9.

Antiresonance and nonlinear systems. Based on the previous results, we are able to extend the linear concepts of antiresonance, stated in Section 2.1, to the nonlinear case, as follows:

- In the case of a conservative system, a nonlinear antiresonance can be defined by the zero of a particular harmonics of a particular nonlinear frequency response of the system. In the case of a damped systems, it is defined as a minimum instead of a zero. This definition is analogous to the one for a linear system, except that it is now related to a given harmonics of the periodic response, and not on the whole response.
- As in the case of a linear system, a nonlinear antiresonance is a local feature of the system, that depends on the driving point, the measurement point and also on the harmonics on which the external force is applied.
- As in the case of a linear system, a minimum of a given harmonics of a given nonlinear frequency response is not necessarily an antiresonance.

- Contrary to the linear case, nonlinear antiresonance cannot be identified to the backbone curve of a dual system, because of the amplitude-frequency dependence. As a consequence, one cannot use traditional backbone (nonlinear mode) numerical continuation to compute it.

3. Numerical continuation

3.1. Problem statement

As stated above, we propose here to define an antiresonance by a zero (conservative system) or, more generally, a minimum (damped system) of a given harmonics amplitude of a given nonlinear frequency response. Antiresonance continuation is thus equivalent to the continuation of a minimum of a frequency response.

The procedure requires an analytical definition of the response amplitude of the jth harmonic measured on the ith degree of freedom and depending on the unknowns of the system (13). A scalar function z is then defined as follows:

$$z = g(\boldsymbol{U}) = \sqrt{x_i^{cj\,2} + x_i^{sj\,2}}. \tag{16}$$

The general framework of the study consists in adding Eq. (16) to the initial system (13) in order to build a new non linear algebraic system:

$$\tilde{\boldsymbol{R}}(\tilde{\boldsymbol{U}}, \omega, f) = \begin{cases} \boldsymbol{R}(\boldsymbol{U}, \omega, f) = 0 & \text{(17a)} \\ z - g(\boldsymbol{U}) = 0, & \text{(17b)} \end{cases}$$

where $\tilde{\boldsymbol{U}} = [\boldsymbol{U}\ z]^\intercal$.

The system (17) is in a convenient form for a wide range of continuation procedures:

- Classical forced response continuation consists in computing a branch of steady-state solutions [35] by imposing f when ω varies, as shown on Fig. 7.
- Backbone curve continuation can be achieved enforcing f and $\boldsymbol{D}$ to zeros while ω is left free. However, the procedure can require to add a phase equation to (17), as explained in [18], since the driving force is zero.
- More specific methods, like bifurcation tracking, consist in following the branch of solution at a given particular point [26] (saddle node, branch point bifurcation ...). For instance, limit point continuation of the Fig. 4 is achieved letting f and ω free and enforcing a constraint, in this case $\frac{\partial \omega}{\partial z} = 0$, as illustrated on Fig. 13.
- The original method that we propose in this paper, namely antiresonance continuation and shown on Figs. 9 and 8, consists in letting free f and ω and enforcing the constraint $\frac{\partial z}{\partial \omega} = 0$, in the case of a damped system. For a conservative system, the constraint is simply $z = 0$.

As it will be seen, this procedure shares similarities with limit point tracking, thus start to recall its strategy before introduce the antiresonance continuation.

3.2. Limit point continuation

As stated before, a limit point is characterized by a vertical tangency of the branch of solution w.r.t. ω at constant f, which leads to

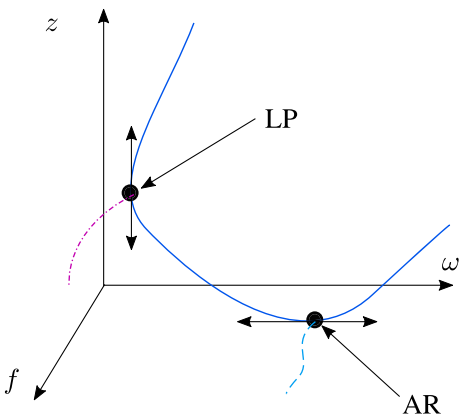

Fig. 13. Branch of solution for constant f (solid line). Limit point continuation (dash-dotted line). Antiresonance continuation (dashed line).

$$\frac{\partial \omega}{\partial z} = 0. \tag{18}$$

Differentiating Eq. (17) w.r.t. ω at constant f yields

$$\frac{\mathrm{d}\tilde{\boldsymbol{R}}}{\mathrm{d}\omega} = \frac{\partial \tilde{\boldsymbol{R}}}{\partial \tilde{\boldsymbol{U}}} \frac{\mathrm{d}\tilde{\boldsymbol{U}}}{\mathrm{d}\omega} + \frac{\partial \tilde{\boldsymbol{R}}}{\partial \omega} = \boldsymbol{0}. \tag{19}$$

Since z is a component of $\tilde{\boldsymbol{U}}$, according to Eq. (18), $\frac{\mathrm{d}\tilde{\boldsymbol{U}}}{\mathrm{d}\omega}$ is then undefined ($\partial z/\partial\omega$ is infinite). Moreover, $\frac{\partial \tilde{\boldsymbol{R}}}{\partial \omega}$ is finite since $\tilde{\boldsymbol{R}}$ depends explicitly on ω (it is in fact non zero because of the time derivatives of the dynamical system (1) that lead, with the HBM, to differentiate the Fourier series and to make ω appear in $\tilde{\boldsymbol{R}}$). Consequently, those two points necessarily imply the singularity of the Jacobian matrix $\tilde{\boldsymbol{J}} = \frac{\partial \tilde{\boldsymbol{R}}}{\partial \tilde{\boldsymbol{U}}}$. The required constraint to carry out the limit point continuation can then be written:

$$\det\left(\tilde{\boldsymbol{J}}\right) = \boldsymbol{0}. \tag{20}$$

Without an analytical expression of $\tilde{\boldsymbol{J}}$, the computation of its determinant may become a numerically cumbersome procedure. For large systems, this can be achieve using the so-called bordering technique where the singularity of $\tilde{\boldsymbol{J}}$ is monitored through the evaluation of a scalar test function [36,37,25]. For smaller systems, an alternative is to use the eigenvector $\tilde{\boldsymbol{\Phi}}_{\boldsymbol{0}}$ associates to a null eigenvalue $\tilde{\lambda}_0 = 0$ of $\tilde{\boldsymbol{J}}$ [38], such as:

$$\det(\tilde{\boldsymbol{J}}) = 0 \Longleftrightarrow \exists \tilde{\boldsymbol{\Phi}}_{\boldsymbol{0}} \neq 0; \quad \tilde{\boldsymbol{J}}\tilde{\boldsymbol{\Phi}}_{\boldsymbol{0}} = \boldsymbol{0}. \tag{21}$$

The final nonlinear algebraic system to solve can be written:

$$\begin{cases} \boldsymbol{R}(\boldsymbol{U}, \omega, f) = \boldsymbol{0} \\ z - g(\boldsymbol{U}) = 0 \\ \tilde{\boldsymbol{J}}\tilde{\boldsymbol{\Phi}}_{\boldsymbol{0}} = \boldsymbol{0} \\ \|\tilde{\boldsymbol{\Phi}}_{\boldsymbol{0}}\| - 1 = 0 \end{cases} \tag{22}$$

It is worth noting that the vector $\tilde{\boldsymbol{\Phi}}_{\boldsymbol{0}}$ is unknown and is normalized by the third equation so that $\tilde{\boldsymbol{\Phi}}_{\boldsymbol{0}} \neq 0$.

At this point, we can summarize the number of unknowns and equations of (22). We have:

$$\dim \boldsymbol{U} = N_{eq}(2H+1), \quad \dim z = 1, \quad \dim \tilde{\boldsymbol{\Phi}}_{\boldsymbol{0}} = \dim \boldsymbol{U} + \dim z, \tag{23}$$

thus a total of $2N_{eq}(2H+1)+4$ unknowns, since ω and f are left free. As usual for continuation procedures, there is a lack a one equation with a total number of $2N_{eq}(2H+1)+3$. Implicit function theorem states that there exists, on a given interval, an implicit parametrization of branches of solutions of (22) as a function of a parameter a [36]. The missing information is thus given by the definition of a and will be provided in Section 4.

3.3. Antiresonance continuation

An antiresonance is characterized by a horizontal tangency of the branch of solution w.r.t. ω at constant f. The basic idea is then to exchange the role of ω and z leading to

$$\frac{\partial z}{\partial \omega} = 0. \tag{24}$$

Based on the limit point continuation procedure, idea is to define formally a new algebraic system $\boldsymbol{R}^*$ from (17) where z becomes the control parameter and ω an unknown

$$\boldsymbol{R}^*(\boldsymbol{U}^*, z, f) = \tilde{\boldsymbol{R}}(\tilde{\boldsymbol{U}}, \omega, f) = \boldsymbol{0}, \tag{25}$$

where $\boldsymbol{U}^* = [\boldsymbol{U}\ \omega]^\mathsf{T}$. Since then, differentiating $\boldsymbol{R}^*$ w.r.t. z yields

$$\frac{\mathrm{d}\boldsymbol{R}^*}{z} = \frac{\partial \boldsymbol{R}^*}{\partial \boldsymbol{U}^*} \frac{\mathrm{d}\boldsymbol{U}^*}{z} + \frac{\partial \boldsymbol{R}^*}{\partial z} = \boldsymbol{0}. \tag{26}$$

Since ω is now a component of $\boldsymbol{U}^*$, according to Eq. (24), $\frac{\mathrm{d}\boldsymbol{U}^*}{\mathrm{d}z}$ is then undefined (because the change of role between ω and z). Moreover, since $\frac{\partial \boldsymbol{R}^*}{\partial z}$ is non zero (because of Eq. (17b), $\boldsymbol{U}^*$ depends explicitly on z), this necessarily implies the singularity of the Jacobian matrix $\boldsymbol{J}^* = \frac{\partial \boldsymbol{R}^*}{\partial \boldsymbol{U}^*}$. The required constraint to carry out the limit point continuation can be written:

$$\det(\boldsymbol{J}^*) = \boldsymbol{0}. \tag{27}$$

Again, it is convenient to replace (27) to obtain:

$$\begin{cases} \boldsymbol{R}(\boldsymbol{U},\omega,f)=\boldsymbol{0} \\ z-g(\boldsymbol{U})=0 \\ \boldsymbol{J}^{*}\boldsymbol{\Phi}_{\boldsymbol{0}}^{*}=\boldsymbol{0} \\ \|\boldsymbol{\Phi}_{\boldsymbol{0}}^{*}\|-1=0 \end{cases} \tag{28}$$

where $\boldsymbol{\Phi}_{\boldsymbol{0}}^{*}$ is the unknown eigenvector associates to the null eigenvalue $\lambda_0^*=0$ of $\boldsymbol{J}^*$.

In the particular case of a conservative system, (28) is simply rewritten:

$$\begin{cases} \boldsymbol{R}(\boldsymbol{U},\omega,f)=\boldsymbol{0} \\ z-g(\boldsymbol{U})=0 \\ z=0 \end{cases} \tag{29}$$

It is also important to point out that Eq. (24) is also true for a maximum of the function z. The procedure describe here is then also suitable for the continuation of a maximum point, like a resonance.

Here again, system (28) comprises $2N_{eq}(2H+1)+4$ unknowns and only $2N_{eq}(2H+1)+3$ equations. It is worth noting that system (25) is just use to build the Jacobian. In practice, $\tilde{\boldsymbol{R}}$ and $\boldsymbol{R}^*$ are identical and Jacobians $\tilde{\boldsymbol{J}}$ and $\boldsymbol{J}^*$ are quite similar, they are given by

$$\tilde{\boldsymbol{J}}=\begin{bmatrix} \frac{\partial \boldsymbol{R}}{\partial \boldsymbol{U}} & \boldsymbol{0} \\ -\frac{\partial g}{\partial \boldsymbol{U}} & 1 \end{bmatrix}, \quad \boldsymbol{J}^{*}=\begin{bmatrix} \frac{\partial \boldsymbol{R}}{\partial \boldsymbol{U}} & \frac{\partial \boldsymbol{R}}{\partial \omega} \\ -\frac{\partial g}{\partial \boldsymbol{U}} & 0 \end{bmatrix}. \tag{30}$$

One observes that only last columns are different so moving from limit point continuation to antiresonance continuation is almost immediate.

4. Numerical solving

In this section, the numerical solving with the Asymptotic Numerical Method (ANM) is presented. System (13) is used as example. ANM is based on a high order perturbation method from an initial solution $(\boldsymbol{U_0},\omega_0,f_0)$ [21,35]. The unknowns of (13) are expanded in a power series as a function of a path parameter a. For instance, a forced steady state computation for fixed f leads to:

$$\begin{cases} \boldsymbol{U}(a)=\boldsymbol{U}_0+a\boldsymbol{U}_1+a^2\boldsymbol{U}_2+\cdots+a^N\boldsymbol{U}_N \\ \omega(a)=\omega_0+a\omega_1+a^2\omega_2+\cdots+a^N\omega_N \\ f=f_0 \end{cases} \tag{31}$$

where f_0 is a constant. The path parameter is defined as the pseudo arc length along the branch of solution [35] and it is defined by:

$$a=(\boldsymbol{U}-\boldsymbol{U}_0)^{\intercal}.\boldsymbol{U}_1. \tag{32}$$

Substituting the power series expansions and the path parameter definition into (13) and equating like powers of a, the coefficients of the series (31) are obtain by solving a succession of linear systems involving a unique tangent matrix. Unlike to predictor–corrector algorithms, where the solution is computed point by point, ANM gives a piecewise continuous representation of the branch of solution parametrized by a. Finally the range of validity of the polynomial approximation is determined *a posteriori* by analysing the residue of (13).

In practice, the periodic solutions of 1 are computed via the tool Manlab 2.0 [27]. The use of this software requires to rewrite the governing equations in a set of first-order differential equations such as:

$$\begin{cases} \dot{\boldsymbol{x}}=\boldsymbol{v} \\ \boldsymbol{M}\dot{\boldsymbol{v}}+\boldsymbol{D}\boldsymbol{v}+\boldsymbol{K}\boldsymbol{x}+\boldsymbol{f}_{nl}(\boldsymbol{v},\boldsymbol{x})=\boldsymbol{F}\cos\omega t. \end{cases} \tag{33}$$

Manlab 2.0 also requires to recast system (33) under the following quadratic form (see Ref. [35] for more details):

$$\boldsymbol{m}(\dot{\boldsymbol{Z}})=\boldsymbol{c}+\boldsymbol{l}(\boldsymbol{Z})+\boldsymbol{q}(\boldsymbol{Z},\boldsymbol{Z}), \tag{34}$$

where the vector of unknowns $\boldsymbol{Z}=[\boldsymbol{x}\ \boldsymbol{v}\ \boldsymbol{u}]^{\intercal}$ contains the original unknown vector $\boldsymbol{x}$, the unknown vector $\boldsymbol{v}$ resulting to the transformation from (1) to (33) and the unknown vector $\boldsymbol{u}$ resulting to the transformation from (33) to (34). $\boldsymbol{c}$ is a constant vector w.r.t. $\boldsymbol{Z}$, $\boldsymbol{l}(-)$ and $\boldsymbol{m}(-)$ are linear operator and $\boldsymbol{q}(-,-)$ is the quadratic operator. For instance, implementation of Eqs. (2) and (3) under the form of (34) is given in Appendix A.1.

Finally, the HBM procedure transform (34) into the pure algebraic system (13) of the form

$$\boldsymbol{R}(\bar{\boldsymbol{U}})=\boldsymbol{C}+\boldsymbol{L}(\bar{\boldsymbol{U}})+\boldsymbol{Q}(\bar{\boldsymbol{U}},\bar{\boldsymbol{U}})=\boldsymbol{0}, \tag{35}$$

where $\bar{\boldsymbol{U}}=[\boldsymbol{U},\omega,f]$ and $\boldsymbol{C},\boldsymbol{L}(-)$ and $\boldsymbol{Q}(-,-)$ are constant, linear and quadratic operators respectively.

One notices that this quadratic framework is particularly suitable for implementation of limit point and antiresonance tracking. If $\tilde{\boldsymbol{R}}$ and $\boldsymbol{R}^*$ are of the form of (35), their jacobians $\tilde{\boldsymbol{J}}$ and $\boldsymbol{J}^*$ are thus linear w.r.t. $\tilde{\boldsymbol{U}}$ and $\boldsymbol{U}^*$ respectively. They can be determined column-wise such as:

$$\tilde{\boldsymbol{J}}\tilde{\boldsymbol{e}}_j = \boldsymbol{L}(\boldsymbol{e}_j) + \boldsymbol{Q}(\tilde{\boldsymbol{U}}, \boldsymbol{e}_j) + \boldsymbol{Q}(\boldsymbol{e}_j, \tilde{\boldsymbol{U}}) \tag{36}$$

and

$$\boldsymbol{J}^*\boldsymbol{e}_j = \boldsymbol{L}(\boldsymbol{e}_j) + \boldsymbol{Q}(\boldsymbol{U}^*, \boldsymbol{e}_j) + \boldsymbol{Q}(\boldsymbol{e}_j, \boldsymbol{U}^*) \tag{37}$$

where $\boldsymbol{e}_j = [0 \ \dots \ 1 \ \dots \ 0]^\intercal$ is a canonical vector where only the jth component equals the unity.

Since then, equations

$$\begin{cases} \tilde{J}\tilde{\boldsymbol{\Phi}}_{\boldsymbol{0}} = \boldsymbol{0} \\ \|\tilde{\boldsymbol{\Phi}}_{\boldsymbol{0}}\| - 1 = 0 \end{cases} \quad \text{and} \quad \begin{cases} \boldsymbol{J}^*\boldsymbol{\Phi}^*_{\boldsymbol{0}} = \boldsymbol{0} \\ \|\boldsymbol{\Phi}^*_{\boldsymbol{0}}\| - 1 = 0 \end{cases}$$

of systems (22) and (28) involve only quadratic operations so procedures described in Sections 3.2 and 3.3 can be easily implemented in the MANLAB 2.0 package.

A critical point is the choice of the initial solution $(\boldsymbol{U}_{\boldsymbol{0}}, \omega_0, f_0)$ which can be computed accurately. This can easily be achieved by carrying out a first classical forced response continuation (by imposing f and letting ω free). Since then, z is computed by substituting power series (31) into Eq. (16) and the value of the path parameter a, corresponding to the desired point of the branch of solution, is computed by solving Eq. (18) (for a limit point) or Eq. (24) (for an extremum) through a Newton–Raphson algorithm [39]. The obtained solution is then used as initial solution of the limit point or extremum continuation procedure.

5. Application to the Euler's pendulum

We now apply concepts presented above to the Euler's pendulum which have the particularity to exhibit both geometric non-linearities and non linear inertial coupling. The system under investigation is then composed of a pendulum whose the center of mass G is subjected to move along a prescribed path $\mathcal{C}$ belonging to a mobile carriage of mass m_c as shown in Fig. 14. The pendulum is considered as a point mass of mass m_p and concentrated at G. The variable X measures the translational displacement of the co-ordinate system $\mathcal{R}_c(O_c, \boldsymbol{x}_c, \boldsymbol{y}_c, \boldsymbol{z}_c)$, attached to the carriage, with respect to the Galilean frame $\mathcal{R}_0(O, \boldsymbol{x}_0, \boldsymbol{y}_0, \boldsymbol{z}_0)$. For the sake of generality, the shape of the trajectory $\mathcal{C}$ is let free with the only condition that it is symmetric along $\boldsymbol{y}_c$. It is therefore convenient to parametrize the displacement of G along $\mathcal{C}$ with the curvilinear abscissa S whose the origin is at the vertex V. The general path shape of $\mathcal{C} : \{G; \theta(S)\}$ is governed by the function $\theta(S)$ which measures the rotation of the Frenet trihedron $\mathcal{R}_F(G, \boldsymbol{t}, \boldsymbol{n}, \boldsymbol{z}_0)$ w.r.t. $\mathcal{R}_c$. The whole system evolves in the gravitational acceleration field $-g\boldsymbol{y}_0$ and the carriage is subjected to an external time-dependent force

$$F(t) = f_0 \cos \omega t, \tag{38}$$

where τ denotes the time. The governing equations can be written

$$(m_c + m_p)\ddot{X} + m_p\ddot{S}\cos\theta - m_p\frac{\mathrm{d}\theta}{\mathrm{d}S}\dot{S}^2\sin\theta = f_0\cos\omega t \tag{39}$$

$$m_p\cos\theta\ddot{X} + m_p\ddot{S} + m_p g\sin\theta + c_p\dot{S} = 0 \tag{40}$$

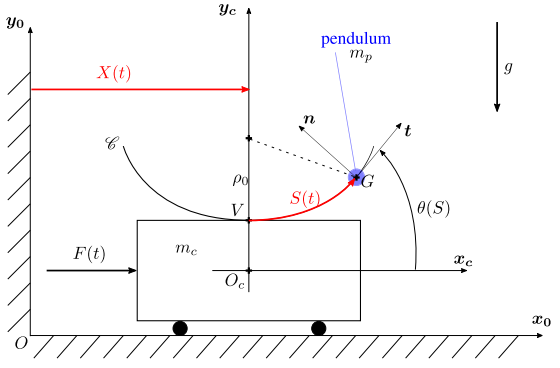

Fig. 14. Investigated Euler's pendulum.

The proof is given in Appendix A.2. Eqs. (39) and (40) stand for the carriage and pendulum dynamics respectively. A viscous damping, of coefficient c_p, has been introduced in Eq. (40). It represents a damping between the pendulum and the carriage along $\mathcal{C}$. One notices the presence of non linear coupling in the mass matrix through the term $\cos\theta$. The nonlinear nature of this inertial coupling vanishes for the particular case where the path $\mathcal{C}$ followed by the center of mass of the pendulum is an horizontal line *i.e.*, $\theta(S) = 0$. In this case, the direction of the gravitational field becomes orthogonal with the pendulum displacement which also causes the vanishing of the stiffness term $m_p g \sin\theta$ of the pendulum in Eq. (40). Obviously, this case has no interest here.

5.1. Free linear vibrations of the uncoupled pendulum

We define here some basic concepts in order to understand how the trajectory $\mathcal{C}$ governs the linear behavior of the pendulum. The carriage of Fig. 14 is assumed fixed w.r.t. $\mathcal{R}_0$ *i.e.*, $X(t)$ is constant. Governing equation of the pendulum is then extracted from Eq. (40) and is given by

$$\ddot{S} + g \sin\theta(S) = 0. \tag{41}$$

The aforementioned symmetry condition about $\mathcal{C}$ implies that $\theta(S) = -\theta(-S)$, so expanding $\sin\theta(S)$ in Taylor's series around S = 0 yields

$$\sin\theta(S) = \left.\frac{\mathrm{d}\theta(S)}{\mathrm{d}S}\right|_{S=0} S + \mathcal{O}(S^3). \tag{42}$$

For a planar curve parametrized as $\mathcal{C}, \theta(S)$ is linked to the curvature $\kappa(S)$ of $\mathcal{C}$ [40] by

$$\frac{\mathrm{d}\theta(S)}{\mathrm{d}S} = \kappa(S) = \frac{1}{\rho(S)}, \tag{43}$$

where $\rho(S)$ is the local radius of curvature of $\mathcal{C}$. When evaluated at $(S = 0)$, Eq. (43) becomes

$$\left.\frac{\mathrm{d}\theta(S)}{\mathrm{d}S}\right|_{S=0} = \kappa_0 = \frac{1}{\rho_0}. \tag{44}$$

where ρ_0 is the radius of curvature of $\mathcal{C}$ at V. From Eq. (44), one sees that the signed curvature κ_0 of $\mathcal{C}$ at the vertex V must be positive *i.e.*, $\left.\frac{\mathrm{d}\theta(S)}{\mathrm{d}S}\right|_{S=0} > 0$ so that Eq. (41) is stable. Therefore in the following, only concave-shaped paths will be considered. Substituting Eq. (44) into (42) and the result into Eq. (41), the linear equation of motion is

$$\ddot{S} + \omega_0^2 S = 0 \tag{45}$$

where $\omega_0 = \sqrt{\frac{g}{\rho_0}}$. One observes that geometric parameter ρ_0 governs the free linear oscillation frequency of the pendulum whatever the shape of the trajectory $\mathcal{C}$, which has not been yet defined.

5.2. Influence of the path shape

We now give a particular shape to the trajectory $\mathcal{C}$. The carriage is still assumed fixed w.r.t. $\mathcal{R}_0$. We address a family of curves, proposed by Denman in [15], whose the intrinsic equation is of the form

$$\rho^2(S) = \rho_0^2 - \lambda^2 S^2 \tag{46}$$

where λ is a parameter governing the path shape. A circle is denoted by $\lambda = 0$ and a cycloid by $\lambda = 1$. Any value in the range $0 < \lambda < 1$ gives an epicycloid, the proof is given in Appendix A.3. Those paths are depicted on Fig. 15 and their corresponding functions $\theta(S)$ are obtained by substituting Eq. (46) into (43), it reads

Circle:

$$\theta(S) = \frac{S}{\rho_0}, \tag{47}$$

Epicycloid:

$$\theta(S) = \frac{1}{\lambda}\operatorname{asin}\frac{\lambda S}{\rho_0}, \tag{48}$$

Cycloid:

$$\theta(S) = \operatorname{asin}\frac{S}{\rho_0}. \tag{49}$$

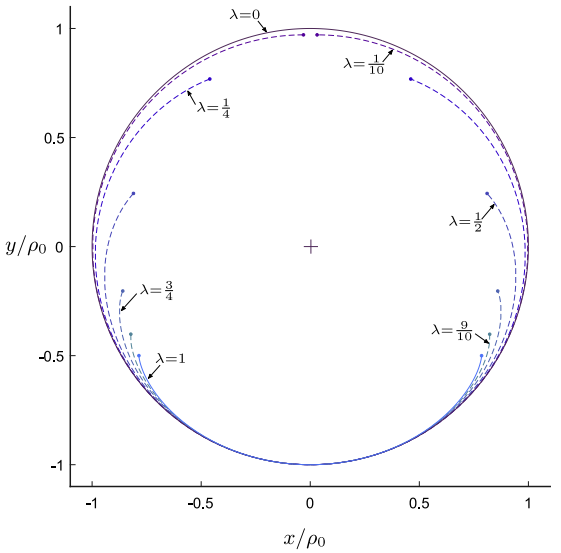

Fig. 15. Evolution of the path shape at a given ρ_0. Circle (solid line, $\lambda = 0$). Epicycloid (dashed lines, $0 < \lambda < 1$). Cycloid (solid line, $\lambda = 1$). • denote cusp points.

Note that the amplitude of the pendulum is bounded by cusp points of epicycloid and cycloid since asin$x$ is defined for $-1 \leqslant x \leqslant 1$.

It is worth noting that substitution of Eq. (49) into (41) gives the linear equation of motion (45). The cycloidal pendulum is known as the Huygens' pendulum [14] for which the free oscillation frequency doesn't depend on the amplitude of oscillations [41]. The cycloid is thus the tautochronic path in the gravitational acceleration field. In the case of the circle and epicycloid, it is of interest to expand the nonlinear term $\sin\theta(S)$ of Eq. (41) in Taylor's series around $S = 0$.

Circle:

$$\sin\theta(S) = \frac{1}{\rho_0}S - \frac{1}{6\rho_0^3}S^3 + \mathcal{O}(S^5). \tag{50}$$

Epicycloid:

$$\sin\theta(S) = \frac{1}{\rho_0}S - \frac{1}{6\rho_0^3}(1-\lambda^2)S^3 + \mathcal{O}(S^5). \tag{51}$$

At third expansion order, we recognize the cubic geometric non-linearity of the Duffing's oscillator addressed in Section 2.2. Coefficient γ governing the magnitude of the geometric non-linearity is given by

Circle:

$$\gamma = -\frac{1}{6\rho_0^3}, \tag{52}$$

Epicycloid:

$$\gamma = -\frac{1}{6\rho_0^3}(1-\lambda^2), \tag{53}$$

Cycloid:

$$\gamma = 0. \tag{54}$$

Since $\gamma < 0$ in the case of circular and epicycloidal pendulums, both exhibit a softening behavior *i.e.*, the free oscillation frequency decreases as the amplitude of oscillation increases. Note also that γ is a function of the parameter λ in Eq. (53). According to the value of λ, the behavior of the epicycloidal pendulum is then more or less soft.

5.3. Results on the full system

We now address the coupled system as described by Eqs. (39) and (40). Different path shapes mentioned before, circle, epicycloid and cycloid, are considered. It is convenient to rewrite the governing equations under the following dimensionless form

$$(1+\mu)x'' + \mu s'' \cos\theta - \mu \frac{\mathrm{d}\theta}{\mathrm{d}s} s'^2 \sin\theta = f\cos\bar{\omega}\tau \tag{55}$$

$$\cos\theta x'' + s'' + \sin\theta + 2\xi_p s' = 0 \tag{56}$$

where

$$\tau = \omega_0 t, \quad (-)' = \frac{\mathrm{d}(-)}{\tau}, \quad \bar{\omega} = \frac{\omega}{\omega_0}, \quad s = \frac{S}{\rho_0}, \quad x = \frac{X}{\rho_0}, \quad \mu = \frac{m_p}{m_c}, \quad \xi_p = \frac{c_p}{2m_p\omega_0}, \quad f = \frac{f_0}{gm_c}. \tag{57}$$

Eqs. (55) and (56) involve the mass ratio μ between the pendulum and the carriage. ξ_p is the damping rate related to the degree of freedom s and involving c_p. The dimensionless amplitude of the external excitation is denoted by f. Implementation of Eqs. (55) and (56) in the form of the quadratic algebraic-differential system (34) is given in Appendix A.4.

The system comprises two linear modes. A first rigid body mode of shape $\Phi_1 = [1 \quad 0]^\intercal$ and associated eigenfrequency $\bar{\omega}_1 = 0$, where the pendulum is locked at $s = 0$, and an oscillating mode $\Phi_2 = [\mu \quad -(1+\mu)]^\intercal$ of associated eigenfrequency $\bar{\omega}_2 = \sqrt{1+\mu}$ which stands for a phase opposition motion between the pendulum and the carriage. In addition, an antiresonance occurs on the carriage response at the free oscillation frequency of the pendulum, $\bar{\omega} = \bar{\omega}_0 = 1$. Fig. 16 depicts the forced response of the system in the case of the circle, epicycloid and cycloid. One observes an amplitude-dependent frequency even in the case of the cycloid: it is thus not the tautochronic path of the coupled system. This is an effect of nonlinear terms on the mass matrix of the system whose the significance is governed by the mass ratio μ. From Eqs. (55) and (56), μ can be viewed as a coupling factor between the pendulum and the carriage.

Fig. 17 shows the forced response as a function of the normalized frequency $\bar{\omega}/\bar{\omega}_2$ at the vicinity of the resonance in the case of a strong coupling *i.e.*, $\mu = 0.5$, a weak coupling *i.e.*, $\mu = 0.25$ and the decoupled pendulum *i.e.*, $\mu = 0$. One sees that the resonance is more and more soft as the parameter μ increases. In the case of a strong coupling, non linear inertial effect overrides geometric non-linearities and exacerbates the softening behavior. In the case of a weak coupling, the inertial coupling becomes negligible and the cycloidal path tends to make the whole system tautochronic.

Fig. 18 shows the convergence of the antiresonance behavior of the system as the number of harmonics H retained in (12) increases. Curves shown in Fig. 18 are the same as those of Fig. 16 but for several amplitudes of excitation. An appropriate number of harmonics must be retained in the solution since the contributions of harmonics higher than H will be neglected through the harmonic balance procedure. When $H = 1$, the solution is not converged and the amplitude-frequency dependence of the antiresonance, in the case of the cycloid, is very weak. By increasing the number of harmonics in the approximation of the solution, one observes a quantitative change for the circle and the epicycloid and a qualitative, from soft to

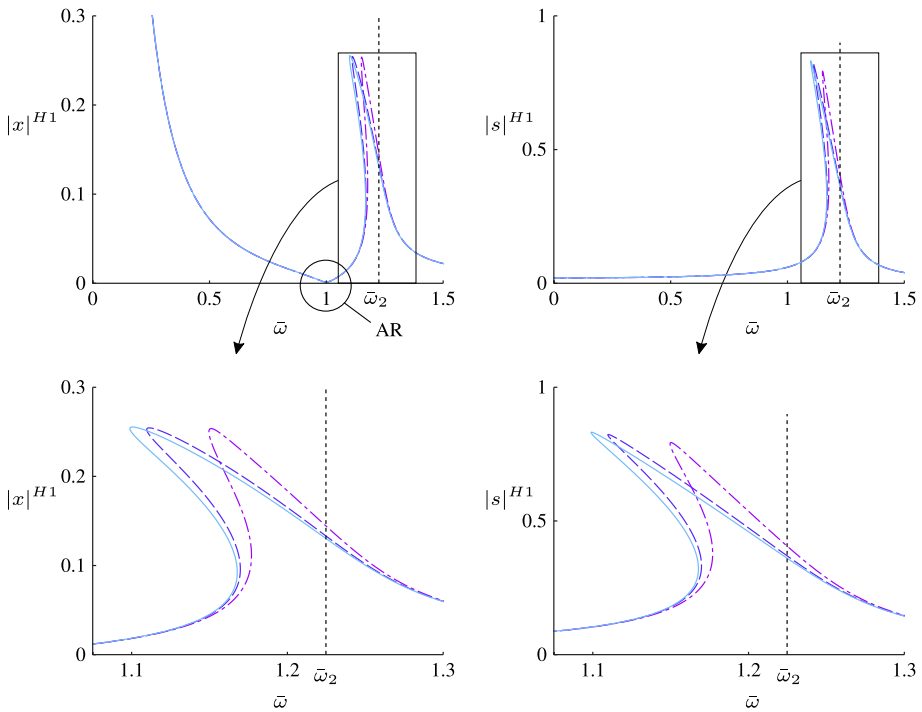

Fig. 16. Evolution of the first harmonic of the carriage response (left) and pendulum displacement (right), in the case of circular (solid line), epicycloidal ($\lambda = 1/2$, dashed line) and cycloidal (dash-dotted line) path. $\mu = 0.5,\ \xi_p = 0.01,\ f = 0.03,\ H = 20$

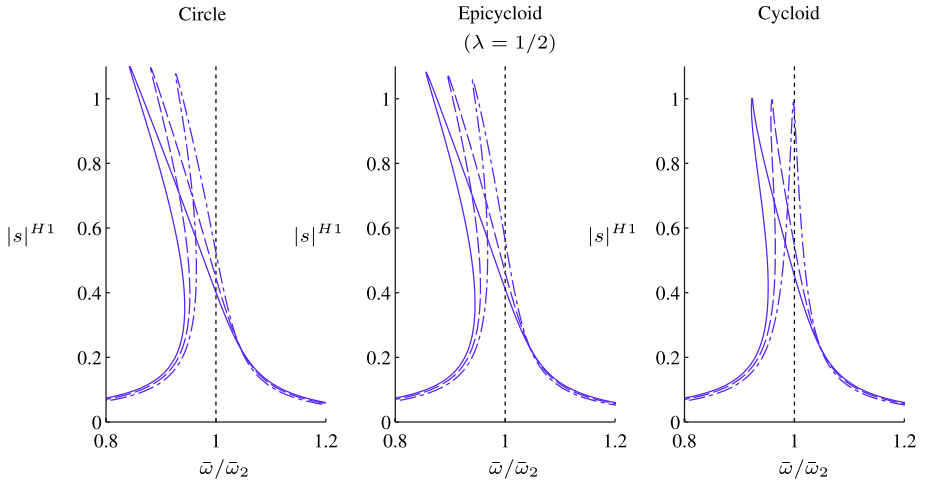

Fig. 17. Evolution of the primary resonance seen on the first harmonic of the pendulum displacement. $f = 0.04$ and $\mu = 0.5$ (solid lines). $f = 0.0315$ and $\mu = 0.25$ (dashed lines). $f = 0.0235$ and $\mu = 0$ (dash-dotted lines). $\xi_p = 0.01$ and $H = 20$.

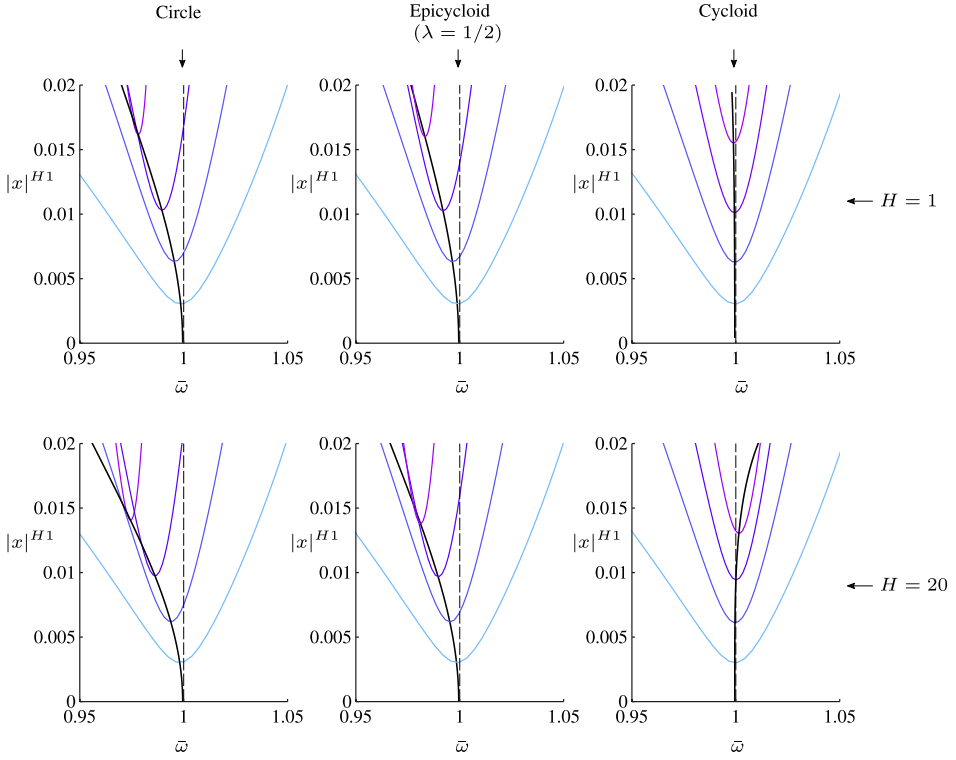

Fig. 18. Evolution of the antiresonance frequency, seen on the first harmonic of the carriage response for several amplitudes of excitation, $f = [0.075; 0.15; 0.225; 0.3]$, $\mu = 0.5$, $\xi_p = 0.01$. Antiresonance continuation is denoted by black solid lines.

hard, for the cycloid. The trend of antiresonance is not the same as that of backbone curve, see Fig. 17 where the cycloid is softening. Here again, nonlinear inertial interactions are involved so the cycloid does not guarantee an amplitude-independent antiresonance curve.

Fig. 19 depicts the forced response, for the cycloidal case, as f increases. For convenience, we chose to represent the response of the carriage in terms of acceleration. One observes the softening behavior of the resonance while the antiresonance exhibits an hardening behavior. At large amplitude of motion, the resonance tends to go stiff leading to bound the location of unstable solutions, represented by the grey area and whose the border is the fold bifurcation continuation. Maximum response amplitude continuation represents the locus of the frequency resonance and one sees that it doesn't

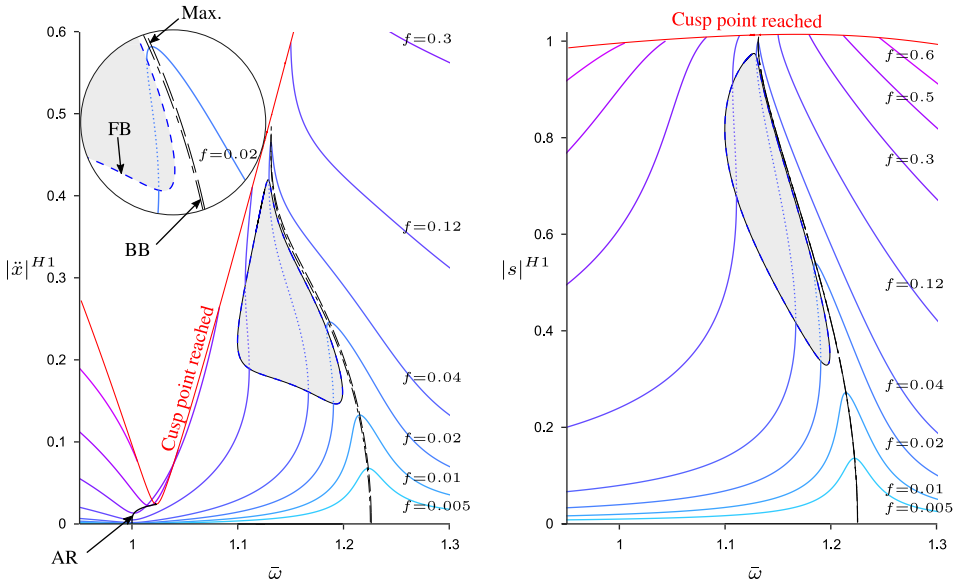

Fig. 19. Evolution of the first harmonic of the carriage response (left) and pendulum displacement (right) in a case of the cycloid. Dashed lines represent unstable solutions. "BB" denotes backbone curve. "FB" stands for fold bifurcation. Maximum response amplitude continuation is denoted "Max" and antiresonance continuation "AR". Parameters values $\mu = 0.5$, $\xi_p = 0.01$ and $H = 20$.

correspond to the eigenfrequency represented by the backbone curve as stated in previous sections. Finally, the maximum amplitude displacement at cusp points *i.e.*, $s(\tau) = 1$ has been computed solving the system (22) since the jacobian $\boldsymbol{J}^*$ is also singular at this particular point.

6. Conclusion

Nonlinear systems are subjected to complex phenomena of various nature and numerical methods such as bifurcation tracking procedures usually assists their design. In this paper, the concept of antiresonance is extended to the nonlinear range and an antiresonance continuation method is proposed with the aim of enhancing the robustness of the development of nonlinear dynamic absorbers. The proposed methodology allows to save up redundant forced steady-state simulations by directly computing the locus of the minimum as well as maximum response amplitude of a given harmonic. Application of the procedure coupled to the harmonic balance method on systems subjected to geometric and/or inertial non-linearities shows the efficiency of the proposed method. In addition, this paper also shows interesting results about the trend of the antiresonance frequency dependence upon the amplitude (hardening or softening), that could be different than that of the nonlinear modes of the system.

Appendix A

A.1. Algebraic-differential system of the Duffing-like system

Implementation of Eqs. (2) and (3) under the form of (34) is given by the following differential-algebraic system:

$$\begin{array}{rcccccc}
\dot{x}_1 & = & & & v_1 & & \\
\dot{x}_2 & = & & & v_2 & & \\
m_1\dot{v}_1 & = & f\cos\omega t & + & c_2(v_2-v_1) - c_1 v_1 - k_1 x_1 + k_2(x_2-x_1) & + & u_1(x_2-x_1) \\
m_2\dot{v}_2 & = & & & c_2(v_1-v_2) + k_2(x_1-x_2) & + & u_1(x_1-x_2) \\
\underbrace{0}_{m(\dot{Z})} & = & \underbrace{\quad}_{c} & & \underbrace{u_1}_{l(Z)} & + & \underbrace{(x_2-x_1)^2}_{q(Z,Z)}
\end{array} \tag{58}$$

where

$$\boldsymbol{Z} = [\underbrace{x_1, x_2}_{\boldsymbol{x}}, \underbrace{v_1, v_2}_{\boldsymbol{v}}, \underbrace{u_1}_{\boldsymbol{u}}]^{\mathsf{T}}. \tag{59}$$

The first two equations of (58) are needed to define additional variables v_1 and v_2 which are used to rewrite (2) and (3) in a set of first-order differential equations (third and fourth equations of (58)). The last equation of (58) is required to define the new unknown u_1 which is required to express nonlinear terms of governing equations under the quadratic formalism of

the operator $\boldsymbol{q}$. Note also that the forcing term $f\cos\omega t$, which is constant w.r.t. unknown vector $\boldsymbol{Z}$, must be put in the operator $\boldsymbol{c}$.

A.2. Governing equations of the Euler's pendulum

We give the methodology to establish governing equations of the Euler's pendulum of the Fig. 14, in the case of a general path $\mathcal{C}$.

The velocity of point G w.r.t. $\mathcal{R}_0$ can be written

$$\boldsymbol{V}_G = \left(\dot{X}\cos\theta(S) + \dot{S}\right)\boldsymbol{t} - \dot{X}\sin\theta(S)\boldsymbol{n}. \tag{60}$$

Total kinetic energy can thus be written

$$\mathcal{T} = \frac{1}{2}\left((m_p + m)\dot{X}^2 + m_p\dot{S}^2 + 2m_p\dot{X}\dot{S}\cos\theta(S)\right), \tag{61}$$

and the potential energy is given by

$$\mathcal{U} = m_p g\int_0^S \sin\theta(S)\mathrm{d}S. \tag{62}$$

Governing Eqs. (39) and (40) are finally obtained applying the Lagrange's equation to kinetic and potential energies such as

$$\frac{\mathrm{d}}{\mathrm{d}\tau}\left(\frac{\partial\mathcal{T}}{\partial\dot{q}_i}\right) - \frac{\partial\mathcal{T}}{\partial q} + \frac{\partial\mathcal{U}}{\partial q} = 0, \tag{63}$$

where $q = [X,\ S]^{\mathrm{T}}$.

A.3. Epicycloid path

Epicycloid $\mathcal{C}$ results from the trajectory of a point G belonging to a generating circle of radius b, rolling without slipping on a base circle of radius a as shown in Fig. 20. Parametric equations of $\mathcal{C}$ are given by

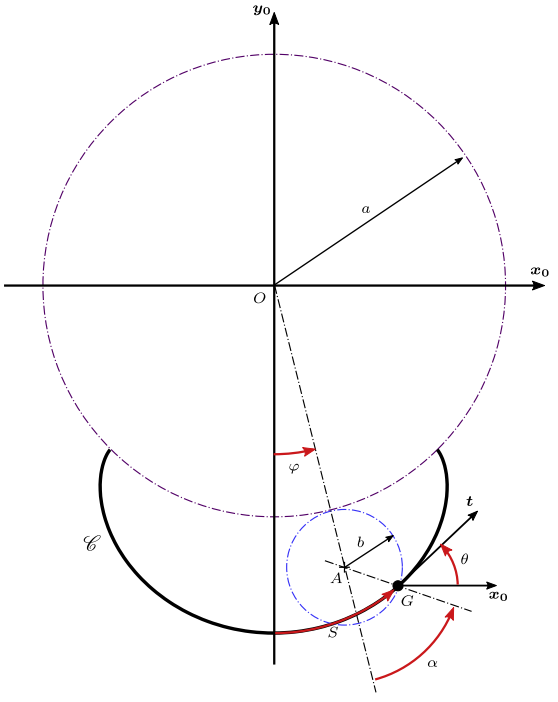

Fig. 20. Epicycloid generation.

$$\boldsymbol{OG} = \begin{cases} (a+b)\sin\varphi + b\sin(\varphi+\alpha) & (64) \\ -(a+b)\cos\varphi - b\cos(\varphi+\alpha) & (65) \end{cases}$$

The rolling without slipping condition leads to

$$\alpha = q\varphi, \tag{66}$$

where $q = \frac{a}{b}$. Parametric Eqs. (64) and (65) can thus be written

$$\begin{cases} x_G = \quad b\Big((q+1)\sin\varphi + \sin(q+1)\varphi\Big) & (67) \\ y_G = -b\Big((q+1)\cos\varphi + \cos(q+1)\varphi\Big) & (68) \end{cases}$$

Transformation from φ to S is done using the fact that

$$\mathrm{d}S^2 = \mathrm{d}x_G^2 + \mathrm{d}y_G^2, \tag{69}$$

By differentiating Eqs. (67, 68) w.r.t. φ and substituting the result in (69), one can write

$$S(\varphi) = \int_0^{\varphi} 2b(q+1)\cos\frac{q}{2}\varphi \ \mathrm{d}\varphi \ = \ 4b\frac{q+1}{q}\sin\frac{q}{2}\varphi. \tag{70}$$

The signed curvature of $\mathcal{C}$, parametrized in Cartesian coordinates, is given by [40]

$$\kappa(\varphi) = \frac{x'_G y''_G - x''_G y'_G}{(x'^2 + y'^2)^{\frac{3}{2}}} \tag{71}$$

where $(-)'$ stands for the derivative of $(-)$ w.r.t. φ. One obtains

$$\kappa(\varphi) = \frac{q+2}{4b(q+1)\cos\frac{q}{2}\varphi}. \tag{72}$$

Substituting (70) into (72) yields

$$\kappa(S) = \frac{q+2}{4b(q+1)\sqrt{1 - \frac{q^2}{16b^2(q+1)^2}S^2}}. \tag{73}$$

The radius of curvature ρ_0 of $\mathcal{C}$ at $S = 0$ is given by

$$\rho_0 = \frac{1}{\kappa(S=0)} = \frac{4b(q+1)}{q+2}. \tag{74}$$

Eq. (73) can thus be rewritten

$$\kappa(S) = \frac{1}{\rho(S)} = \frac{1}{\rho_0\sqrt{1 - \frac{\lambda^2}{\rho_0^2}S^2}} \tag{75}$$

where $\lambda = \frac{q}{q+2}$. Finally, using the fact that [40]

$$\theta(S) = \int_0^S k(S)\mathrm{d}S \tag{76}$$

the tangent angle θ can be written

$$\theta(S) = \frac{1}{\lambda}\mathrm{asin}\frac{\lambda S}{\rho_0}. \tag{77}$$

Since the function $\sin^{-1}x$ is defined in the interval $-1 \leqslant x \leqslant 1$, we can deduce from (77) the maximal value S_{max} of S as

$$S_{max} = \frac{\rho_0}{\lambda}. \tag{78}$$

In addition, the rewrite of Eq. (77) w.r.t. the normalized displacement $\bar{S}$ yields

$$\theta(\bar{S}) = \frac{1}{\lambda}\operatorname{asin}\lambda\bar{S}. \tag{79}$$

where $\bar{S} = S/\rho_0$. This shows that the parameter λ governs the general shape of the epicycloid at a given ρ_0. On the other hand, at given lambda, a scaling factor applied to ρ_0 causes the translation of the curve along $\boldsymbol{y_0}$.

A.4. Algebraic-differential system of the Euler's pendulum

The quadratic differential-algebraic system of the Euler's Pendulum implemented in the MANLAB package can be written:

$$\begin{array}{ccccccc}
\ddot{x} & + & 0 & - & A_x & + & 0 \\
\dot{s} & + & 0 & - & V_s & + & 0 \\
\dot{V}_s & + & 0 & - & A_s & + & 0 \\
0 & - & f & + & (1+\mu)\,A_x & + & \mu\,(A_sC_\theta - \alpha\beta) \\
0 & + & 0 & + & A_s + 2\xi_p V_s & + & A_xC_\theta \\
0 & + & 0 & + & \alpha & - & \delta V_s \\
0 & + & 0 & + & \beta & - & S_\theta V_s \\
0 & - & 1 & + & 0 & + & \rho\delta \\
0 & - & 1 & + & \rho & + & \lambda^2 s^2 \\
0 & + & 0 & - & \rho & + & \eta^2 \\
0 & + & 0 & + & C_\theta - g_c(s) & + & 0 \\
0 & + & 0 & + & S_\theta - g_s(s) & + & 0 \\
\underbrace{} & & \underbrace{} & & \underbrace{} & & \underbrace{} \\
m(\dot{Z}) & & c & & l(Z) & & q(Z,Z)
\end{array} = 0, \tag{80}$$

where $\boldsymbol{Z} = [\boldsymbol{x}\ \boldsymbol{v}\ \boldsymbol{u}]^\intercal$. $\boldsymbol{x} = [\dot{x}\ s]^\intercal$ is the original vector of unknowns of governing Eqs. (55) and (56). $\boldsymbol{v} = [V_s\ A_x\ A_s]^\intercal$ is the vector of additional variables resulting from the transformation of governing equations in a set of first-order differential equations. $\boldsymbol{u} = [\alpha\ \beta\ \delta\ \rho\ \eta\ C_\theta\ S_\theta]^\intercal$ is the vector of additional variables resulting from the quadratic recasting of first-order differential equations. One notices that system (80) involves, in the two last equations, functions $g_c(s)$ and $g_s(s)$ which respectively stand for $\cos\theta(s)$ and $\sin\theta(s)$. Using path functions give by Eqs. (47)–(49), $g_c(s)$ and $g_s(s)$ can be written:

Circular path ($\lambda = 0$):

$$g_c(s) = \cos s, \quad g_s(s) = \sin s. \tag{81}$$

Epicycloidal path ($\lambda = \frac{1}{2}$):

$$g_c(s) = 1 - \lambda s^2, \quad g_s(s) = s\sqrt{1-\lambda^2 s^2} = s\eta. \tag{82}$$

Cycloidal path ($\lambda = 1$):

$$g_c(s) = \sqrt{1-\lambda^2 s^2} = \eta, \quad g_s(s) = s. \tag{83}$$

where $\eta = \sqrt{\rho(s)}$. Note that (82) and (83) are quadratic equations and can therefore be directly implemented in (80). For the circular path, $g_c(s)$ and $g_s(s)$ are non-polynomial nonlinear functions which is non suitable for the MANLAB formalism. However, Karkar has proposed a quadratic frame to deal with non-polynomial non-linearities of various nature [42]. In this paper, trigonometric functions $\cos s$ and $\sin s$ of the circular pendulum were expanded in Taylor series up to $\mathcal{O}(s^{10})$ and $\mathcal{O}(s^{11})$ respectively which consequently implies the introduction of new additional variables in (80).

References

[1] R.A. Ibrahim, Recent advances in nonlinear passive vibration isolators, J. Sound Vib. 314 (3) (2008) 371–452.
[2] H. Frahm, Device for damping vibrations of bodies., U.S. Patent 989958.
[3] R. Viguié, G. Kerschen, Nonlinear vibration absorber coupled to a nonlinear primary system: a tuning methodology, J. Sound Vib. 326 (3) (2009) 780–793.
[4] G. Habib, T. Detroux, R. Viguié, G. Kerschen, Nonlinear generalization of den hartog's equal-peak method, Mech. Syst. Signal Process. 52–53 (Supplement C) (2015) 17–28.
[5] A. Vakakis, O. Gendelman, L. Bergman, D. McFarland, G. Kerschen, Y. Lee, Nonlinear Targeted Energy Transfer in Mechanical and Structural Systems, Solid Mechanics and Its Applications, Springer, Netherlands, 2008.
[6] E. Gourdon, N. Alexander, C. Taylor, C. Lamarque, S. Pernot, Nonlinear energy pumping under transient forcing with strongly nonlinear coupling: theoretical and experimental results, J. Sound Vib. 300 (3) (2007) 522–551.
[7] B. Vaurigaud, L. Manevitch, C.-H. Lamarque, Passive control of aeroelastic instability in a long span bridge model prone to coupled flutter using targeted energy transfer, J. Sound Vib. 330 (11) (2011) 2580–2595.
[8] O.V. Gendelman, Targeted energy transfer in systems with non-polynomial nonlinearity, J. Sound Vib. 315 (3) (2008) 732–745.
[9] E. Gourc, G. Michon, S. Seguy, A. Berlioz, Targeted energy transfer under harmonic forcing with a vibro-impact nonlinear energy sink: Analytical and experimental developments, J. Vib. Acoust. 137 (3) (2015).

[10] J.P. Den Hartog, Stephen Timoshenko 60th Anniversary, Macmillan, New York, 1938.
[11] D.E. Newland, Nonlinear aspects of the performance of centrifugal pendulum vibration absorbers, ASME, J. Eng. Industry 86 (1964) 257–263.
[12] M. Sharif-Bakhtiar, S.W. Shaw, Effects of nonlinearities and damping on the dynamic response of a centrifugal pendulum absorber, ASME, J. Vib. Acoust. 114 (1992) 305–311.
[13] E. Rodgers, Brachistochrone and tautochrone curves for rolling bodies, Am. J. Phys. 14 (1946) 249–252.
[14] C. Huygens, Horologuium oscilatorium sive de motu pendularium, Paris, 1673.
[15] H. Denman, Tautochronic bifilar pendulum torsion absorbers for reciprocating engines, J. Sound Vib. 159 (1992) 251–277.
[16] A.H. Nayfeh, D.T. Mook, Nonlinear Oscillations, John Wiley & Sons, 1979.
[17] G. Kerschen, Computation of Nonlinear Normal Modes through Shooting and Pseudo-Arclength Computation, Springer, Vienna, 2014, pp. 215–250.
[18] S. Karkar, B. Cochelin, C. Vergez, A comparative study of the harmonic balance method and the orthogonal collocation method on stiff nonlinear systems, J. Sound Vib. 333 (12) (2014) 2554–2567.
[19] E.J. Doedel, B.E. Oldeman, Auto-07p: continuation and bifurcation software for ordinary differential equations, 1998. URL http://indy.cs.concordia.ca/auto.
[20] A. Dhooge, W. Govaerts, Y.A. Kuznetsov, Matcont: a matlab package for numerical bifurcation analysis of odes, ACM Trans. Math. Softw. 29 (2) (2003) 141–164.
[21] B. Cochelin, A path-following technique via an asymptotic-numerical method, Comput. Struct. 53 (5) (1994) 1181–1192.
[22] G. Habib, G. Kerschen, A principle of similarity for nonlinear vibration absorbers, Physica D 332 (2016) 1–8.
[23] H. Liao, W. Wu, D. Fang, The reduced space sequential quadratic programming (sqp) method for calculating the worst resonance response of nonlinear systems, J. Sound Vib. 425 (2018) 301–323.
[24] H. Liao, Global resonance optimization analysis of nonlinear mechanical systems: application to the uncertainty quantification problems in rotor dynamics, Commun. Nonlinear Sci. Numer. Simul. 19 (9) (2014) 3323–3345.
[25] T. Detroux, L. Renson, L. Masset, G. Kerschen, The harmonic balance method for bifurcation analysis of large-scale nonlinear mechanical systems, Comput. Methods Appl. Mech. Eng. 296 (Supplement C) (2015) 18–38.
[26] L. Xie, S. Baguet, B. Prabel, R. Dufour, Bifurcation tracking by harmonic balance method for performance tuning of nonlinear dynamical systems, Mech. Syst. Signal Process. 88 (Supplement C) (2017) 445–461.
[27] R. Arquier, S. Karkar, A. Lazarus, O. Thomas, C. Vergez, B. Cochelin, Manlab 2.0: an interactive path-following and bifurcation analysis software, 2005, Technical report, URL http://manlab.lma.cnrs-mrs.fr.
[28] J. Shaw, S.W. Shaw, A.G. Haddow, On the response of the non-linear vibration absorber, Int. J. Non-Linear Mech. 24 (4) (1989) 281–293.
[29] M.A. Acar, S.W. Shaw, B.F. Feeny, Nonlinear dynamics of flexible rotating shafts with centrifugal pendulum vibration absorbers, in: ASME 2015 International Design Engineering Technical Conferences and Computers and Information in Engineering Conference, American Society of Mechanical Engineers, 2015, pp. V008T13A077–V008T13A077.
[30] M. Géradin, D. Rixen, Mechanical Vibrations: Theory and Applications to Structural Dynamics, J, Wiley & Sons, 1997.
[31] W. Feng-Quan, H. Xiao-Ling, G. Ying-Zheng, Analysis of the characteristics of pseudo-resonance and anti-resonance, J. Vib. Acoust. 118 (4) (1996) 663–667.
[32] F. Wahl, G. Schmidt, L. Forrai, On the significance of antiresonance frequencies in experimental structural analysis, J. Sound Vib. 219 (3) (1999) 379–394.
[33] G. Duffing, Erzwungene Schwingungen bei veränderlicher Eigenfrequenz und ihre technische Bedeutung, no. 41–42, R, Vieweg & Sohn, 1918.
[34] A. Lazarus, O. Thomas, A harmonic-based method for computing the stability of periodic solutions of dynamical systems, Comptes Rendus Mécanique 338 (9) (2010) 510–517.
[35] B. Cochelin, C. Vergez, A high order purely frequency-based harmonic balance formulation for continuation of periodic solutions, J. Sound Vib. 324 (12) (2009) 243–262.
[36] R. Seydel, Practical Bifurcation and Stability Analysis, third ed., Interdiciplinary Applied Mathematics, vol. 5, Springer, 2010.
[37] W.J.F. Govaerts, Numerical Methods for Bifurcations of Dynamical Equilibria, Society for Industrial and Applied Mathematics, 2000.
[38] S. Baguet, B. Cochelin, Determination of branches of limit points by an asymptotic numerical method, European Congress on Computational Methods in Applied Sciences and Engineering.
[39] W.H. Press, S.A. Teukolsky, W.T. Vetterling, B.P. Flannery, Numerical Recipes 3rd Edition: The Art of Scientific Computing, Cambridge University Press, 2007.
[40] M. do Carmo, Differential Geometry of Curves and Surfaces, Prentice-Hall, 1976.
[41] G. Baker, J. Blackburn, The Pendulum: A Case Study in Physics, Oxford University Press, 2009.
[42] S. Karkar, B. Cochelin, C. Vergez, A high-order, purely frequency based harmonic balance formulation for continuation of periodic solutions: the case of non-polynomial nonlinearities, J. Sound Vib. 332 (4) (2013) 968–977.